Solid State Laboratory
Research Triangle Institute
Post Office Box 490
Durham, North Carolina 27702

DIFFUSION PROCESS MODELING

Contract No. NAS8-11243

January 1965

Robert P. Donovan

Technical Summary Report

May 1964 to December 1964

Prepared for

George C. Marshall Space Flight Center
Astrionics Laboratory
National Aeronautics and Space Administration
Huntsville, Alabama 35812

Foreword

This summary report was prepared by the Solid State Laboratory of the Research Triangle Institute under Contract No. NAS8-11243, "Improving Silicon Integrated Device Reliability by Modeling the Processes of Fabrication. I. Diffusion." The work began in May 1964, ended in December 1964, and was administered under the technical direction of the Astrionics Laboratory of the George C. Marshall Space Flight Center. Dr. A. M. Holladay was technical supervisor for the Laboratory.

Abstract

The objective of the program initiated by this contract is the development of relationships between the electrical properties of silicon devices and the variables of the processes by which these devices were fabricated. The initial experiments, described in this summary report, consider only the influence of the variables of a specific diffusion process upon: 1) the junction depth and sheet resistivity of the diffused layer, and 2) the reverse current and the breakdown voltage of a planar diode so formed. The relationships derived are:

$$\hat{x}_j = 1.364 \times 10^7 \; t^{0.66} \; e^{-\frac{14750}{T}} \; (\ln c - 0.52)$$

$$\hat{\rho}_s = \frac{1.647 \times 10^4 \; t^{-1.4} \; e^{\frac{5000}{T}}}{c(\ln c - 0.5)}$$

$$\ln \hat{V}_{(BR)} = 5.005 + 0.032 \ln t - \frac{2084}{T}$$

$$\ln \hat{I}_R = 9.27 + 0.21 \; x_j \rho_s$$

where x_j = junction depth (A)

ρ_s = sheet resistivity (ohms/□)

$V_{(BR)}$ = breakdown voltage (at a reverse current of 200 μa)

I_R = reverse current (at a reverse voltage of 10 volts μa)

t = time of diffusion (minutes)

T = temperature of diffusion (°K)

c = impurity concentration during diffusion (ppm)

The expression for $\hat{x}_j$ is judged to be adequate, while that for $\hat{\rho}_s$ is adequate only at the highest values of c. The expressions for both $V_{(BR)}$ and I_R are inadequate.

Table of Contents

Section		Page
1.	Introduction	1
2.	Model Development	7
	2.1 Solution to the Diffusion Equation for Finite Rate Limitation	8
3.	Experimental Work	18
4.	Data Evaluation	33
5.	Conclusions and Recommendations	53
	References	56

List of Illustrations

Figure		Page
1	Sub-dividing blocks in the modeling of system electrical performance	2
2	Solutions to Eq. 13, presented as plots of $G \equiv N_B/N_{eq}$ against $a \equiv x_j/2\sqrt{Dt}$	10
3	Solutions to Eq. 13, presented as plots of $J \equiv \bar{N}/N_B$ against $a \equiv x_j/2\sqrt{Dt}$	11
4	Gas flow schematic for phosphine diffusion	19
5	Photomask for defining areas of diffusion	23
6	Photomask for defining areas of ohmic contact	25
7	Wafer following processing	28
8	Photomicrograph of units on a completed wafer	29
9	Schematic of measuring circuit for diode electrical properties	32
10	Junction depth predicted by Eq. 35 as a function of phosphine concentration during diffusion	36
11	Junction depth predicted by Eq. 35 as a function of diffusion temperature	37
12	Junction depth predicted by Eq. 35 as a function of diffusion time	38
13	Distribution of residuals from Eq. 35 and the top surface data of Table 1	39
14	A comparison of sheet resistivity as predicted by Eq. 36 and that observed (aveg. top surface data, Table 1) for the lower values of impurity concentration	42
15	A comparison of sheet resistivity as predicted by Eq. 36 and that observed (aveg. top surface data, Table 1) for the highest value of impurity concentration	44

List of Illustrations (Continued)

Figure		Page
16	A comparison of sheet resistivity as predicted by Eq. 43 and that observed (aveg. top surface data, Table 1) for the highest value of impurity concentration	45
17.	Typical diode I-V characteristics	49

List of Tables

		Page
Table 1	Raw Data from First Diffusion Experiment	34
Table 2	Residuals Calculated from the Observed Sheet Resistivity (Aveg. Top Surface Data, Table 1) and the Predicted (Eq. 36)	41
Table 3	Raw Data from Second Diffusion Experiment	48

1. Introduction

The work described in this summary report is the initial step of a program whose goal is the development of mathematical expressions relating the electrical performance of a silicon device to the significant parameters of its fabrication. In principle the performance of the device under fixed test conditions should depend only on these variables but at present the functional form of the dependence can only be qualitatively stated and with reservations. The purpose of the present phase is to furnish explicit mathematical statements, relating various measures of electrical performance to the significant independent material and processing variables, whatever they may prove to be.

The overall task becomes simpler when broken into steps as shown in Figure 1. The list of variables included in block 1 is, of course, incomplete and the identity of all significant variables that must be included there is, in fact, a major problem. Ideally block 1 should be a complete listing of all important, independent variables, describing the starting material and the processes through which the starting material is passed in being manufactured into a device. It is convenient at first to treat such variables as resistivity, lifetime, dislocation density, etc., as independent variables. Other variables such as surface finish, surface contamination, impurity compensation, trace impurities, etc., may well be quite important but are being neglected until their need is clearly evident.

The processing variables of block 1 include all those which are independently controlled in the fabrication of the device. Even for simple structures the number of such independent process variables can

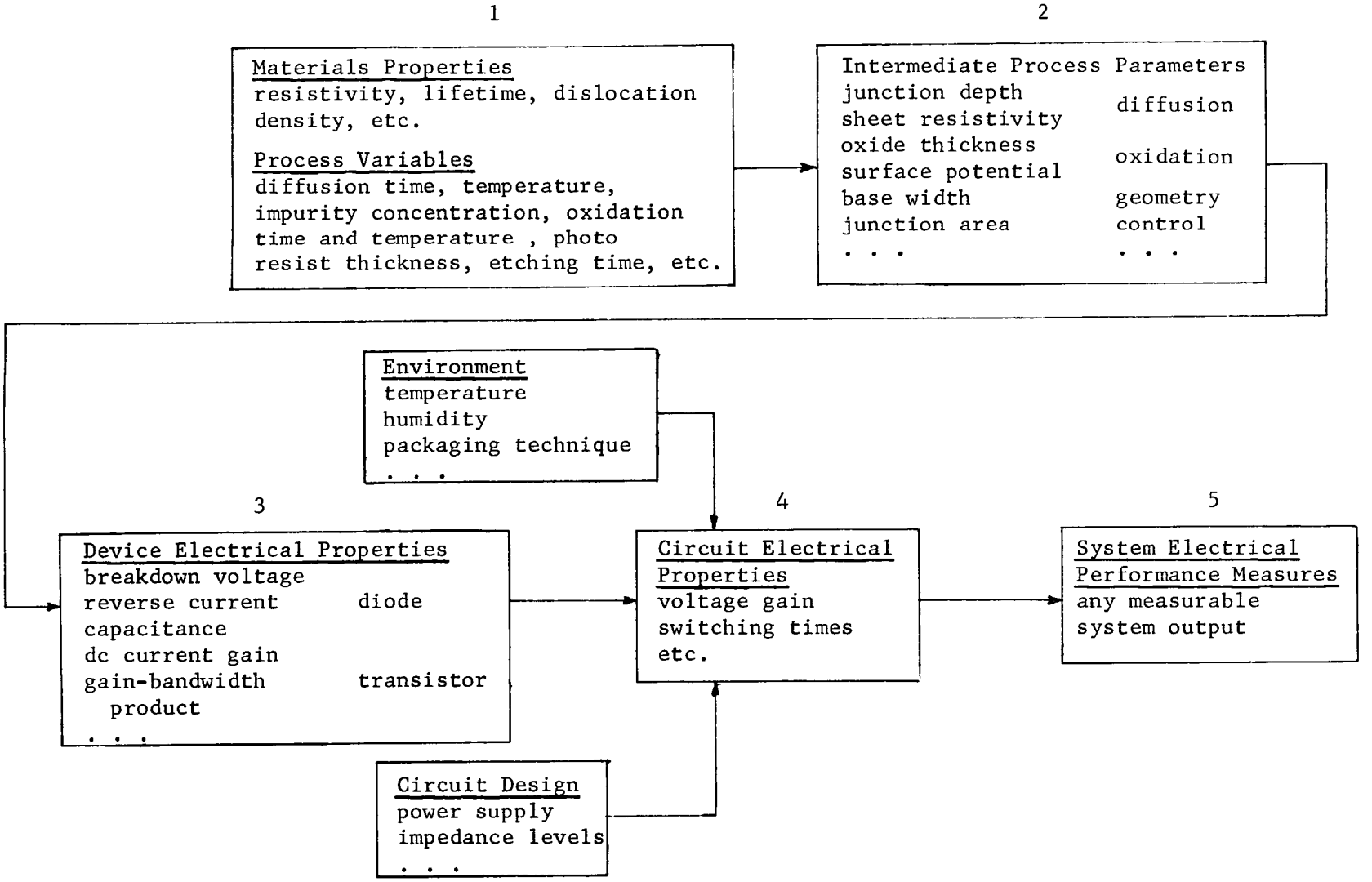

Fig. 1. Sub-dividing blocks in the modeling of system electrical performance

be quite large when all the various processes are accounted for. The specific variables measured may differ with the specific technique used; for example, the variables of oxidation performed in a wet oxygen system must include the oxygen flow rate and the water bath temperature in addition to the time and temperature of oxidation, while oxidation using a steam system is determined completely by the time and temperature of the oxidation. To divorce the results of the experimental work of this program from the specific techniques used, intermediate process parameters are introduced in block 2. These parameters are measurable numbers whose values depend upon the independent variables of the process with which they are associated. Junction depth and sheet resistivity, for example, are two intermediate process parameters of diffusion whose values are dependent upon the independent variables of the diffusion technique employed. These independent variables of diffusion are not the same for a one-step process, as they would be for a two-step process or a third type diffusion process, but the diffused layers they describe are assumed to be the same regardless of how they are obtained.

The listing of intermediate process parameters is complete when all the device electrical properties of interest (block 3, Fig. 1) can be adequately expressed in terms of the process parameters of block 2, Fig. 1. In addition, the mathematical relationships between the dependent variables of block 2 and the independent variables of block 1 are empirically less complex than those between block 1 and block 3. Part of the reason for this observation may be that the dependent properties of block 3 are simply much more sensitive to changes in the variables of block 1 than are the measured parameters of block 2.

The properties to be included in blocks 3, 4, and 5 of Fig. 1 depend upon specific applications, requiring specific properties. Beyond block 3, variables describing circuit design and environment become important.

For the present work, only a small number of variables from each of the first three blocks have been chosen. Using a phosphine gas-source diffusion system [Ref. 1], wafers of p-type silicon, cut from the same ingot, have been diffused under conditions selected for investigating three of the independent variables of diffusion--time t, temperature T, and impurity concentration c. These three variables are the only independent variables of the experiment; all other material properties and process parameters have been held constant, as best as can be determined. The diffused wafers were cut from the same ingot, prepared for diffusion by identical procedures, and evaluated with the same test equipment and personnel.

Two sets of dependent variables were measured: (1) junction depth (x_j) and sheet resistivity (ρ_s) of a diffused layer, (2) junction reverse current I_R (at a reverse bias of 10 V) and junction breakdown voltage $V_{(BR)}$ of planar diodes formed during the same diffusion. The latter measurements were made at a temperature of 200°C and $V_{(BR)}$ at a reverse current of 200 μa.

The first set of measured data (x_j and ρ_s) yields information relating the independent variables of block 1 (t, T, and c) and those of block 2:

$$x_j = x_j(t,T,c) \qquad (1)$$

$$\rho_s = \rho_s(t,T,c) \tag{2}$$

The second set of data measurements gives both:

$$I_R = I_R(\rho_s,\ x_j) \tag{3}$$

$$V_{(BR)} = V_{(BR)}(\rho_s,\ x_j) \tag{4}$$

and

$$I_R = I_R(t,T,c) \tag{5}$$

$$V_{(BR)} = V_{(BR)}(t,T,c) \tag{6}$$

Relationships (1) and (2) are unique for the diffusion system investigated here; relationships (3) and (4) could be general and independent of the diffusion system. The word "could" is used to suggest that other intermediate diffusion variables (impurity graident, for example) may be required before relationships between blocks 2 and 3 are adequate. Once these relationships are established, however, the results are independent of any particular technique. The differences in controlling diffusion by a one-step or a two-step process, geometry by photoengraving or an electron beam appear only in the relationships between block 1 and block 2. Beyond block 2 process differences are expected to disappear.

At the same time the relative quality of competing processes can be evaluated objectively by comparing the predictability (as measured, say, by the standard deviations) of the dependent variables in block 2 as obtained by the different processes. No such comparison has been attempted so far; the single step diffusion process has been investigated

exclusively--primarily because of the small number of well identified, easily measured variables which seem to permit good reproducibility of the diffusions.

The procedure by which relationships (1), (2) and (3), (4) or (5), (6) are obtained is semi-empirical. Theoretical relationships are derived a priori, based on known information in the open literature. Data are fitted to these relationships by a technique such as least squares. The judgment that the relationship obtained by this procedure is adequate is made by comparing the uncertainties in prediction with those expected in other steps of the processing.

The following sections summarize the development of models describing phosphine source diffusion and the electrical properties of planar diodes fabricated from such diffused layers in terms of the time, temperature and impurity concentration during diffusion. Theoretical models are derived in Sec. 2 and the results of statistical curve fitting from the data are presented in Sec. 4. Sec. 3 describes the experimental technique for fabricating diffused diodes and gathering the data. Conclusions and recommendations for follow-up work are outlined in Sec. 5.

2. Model Development

Solutions to Fick's second law of diffusion have been calculated by various authors for various boundary conditions [Refs. 2, 3]; typically these solutions are to the one dimensional form of the diffusion equation:

$$\frac{\partial N}{\partial t} = D \frac{\partial^2 N}{\partial x^2} \quad , \tag{7}$$

where N is the concentration of the diffusing species, t is time, x is distance measured along the direction of diffusion, and D is the diffusion coefficient which has been assumed to be independent of x. The boundary conditions most often of interest are those in which either:

1. The surface concentration remains constant throughout the diffusion:

$$N(x,0) = 0 \quad \text{for} \quad x > 0 \ ,$$

$$N(0,t) = N_o \quad \text{for} \quad t \geq 0 \ .$$

The solution is the complementary error function:

$$N = N_o \ \text{erfc} \ \frac{x}{2\sqrt{Dt}} \quad , \tag{8}$$

or

2. The flow of impurity across the boundary (x = 0) is zero:

$$N(x,0) = 0 \quad \text{for} \quad x > 0 \ ,$$

$$\left.\frac{\partial N}{\partial x}\right|_{x = 0} = 0 \ .$$

The solution is the gaussian distribution:

$$N = \frac{Q}{\sqrt{\pi Dt}} \exp\left(\frac{x^2}{4Dt}\right) , \qquad (9)$$

where Q is the total number of impurities per unit area contained in a thin planar sheet adjacent to x = 0.

These two cases represent extremes among the possible rate limitations that can occur at the surface. Constant surface concentration during diffusion (case 1) implies no rate limitation whatsoever; no impurity flow across the surface (case 2) corresponds to maximum rate limiting at the surface. In reality the surface rate limitation is most likely somewhere between these two extremes. Smits [Ref. 3] has shown, however, that the differences in impurity distributions arising from even the two extremes of rate limitation is so small as to be negligible for all practical purposes. And indeed the usual procedure is to assume one extreme or the other, using either the complementary error function or the gaussian function to describe the impurity distribution following diffusion. It is the purpose of this section to investigate solutions in which the rate limitation at the surface is not neglected in an effort to predict more accurately the effects that are seen during phosphorus diffusion at low values of local impurity concentration c.

2.1 Solution to the Diffusion Equation for Finite Rate Limitation

Impurity diffusion into silicon takes place through a surface plane, taken as x = 0 in the following discussion. The number of impurities arriving at the surface from either a gas phase or a liquid/solid oxide is assumed, after Smits, to be proportional to the difference between the actual surface concentration N_o and the equilibrium concentration N_{eq}. The equilibrium concentration is the impurity concentration

reached as diffusion time $t \rightarrow \infty$; N_{eq} should depend on the impurity concentration in the phase adjacent to the silicon surface through which diffusion is proceeding. The boundary condition at this surface can be written as:

$$K[N_{eq} - N(0,t)] = -D \left.\frac{\partial N(x,t)}{\partial x}\right|_{x = 0} . \qquad (10)$$

With such a boundary condition the solution to Eq. 7 becomes [Ref. 3]:

$$N(y,z) = N_{eq} \left[\operatorname{erfc}(y) - e^{(y + z)^2 - y^2} \operatorname{erfc}(y + z)\right] , \qquad (11)$$

where

$$y = \frac{x}{2\sqrt{Dt}} \quad \text{and} \quad z = \frac{K}{D}\sqrt{Dt} = K\sqrt{t/D} .$$

Solutions to this equation are plotted graphically in Figs. 2 and 3.

To obtain the net impurity concentration the background impurity concentration (assumed to have remained uniform during the diffusion) must be subtracted from the diffused impurity concentration given in Eq. 11:

$$\eta(y,z) = N(y,z) - N_B$$

$$= N_{eq} \left[\operatorname{erfc}(y) - e^{(y + z)^2 - y^2} \operatorname{erfc}(y + z)\right] - N_B \qquad (12)$$

The metallurgical junction between a diffusing species and the uniform background impurities occurs at $\eta(y,z) = 0$ or

$$\frac{N_B}{N_{eq}} = \operatorname{erfc}(y_j) - e^{2y_j z + z^2} \operatorname{erfc}(y_j + z) \equiv G \qquad (13)$$

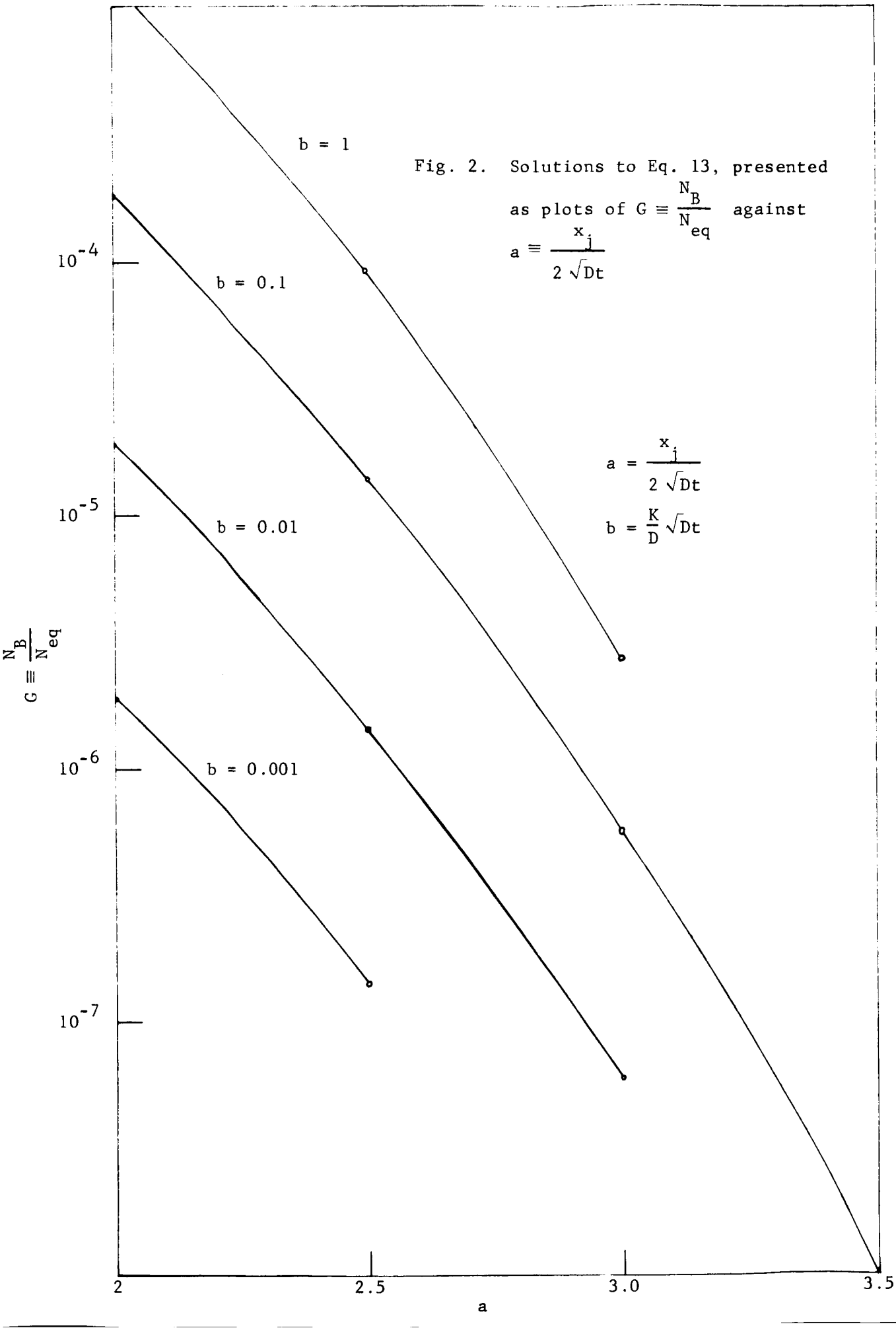

Fig. 2. Solutions to Eq. 13, presented as plots of $G \equiv \frac{N_B}{N_{eq}}$ against $a \equiv \frac{x_j}{2\sqrt{Dt}}$

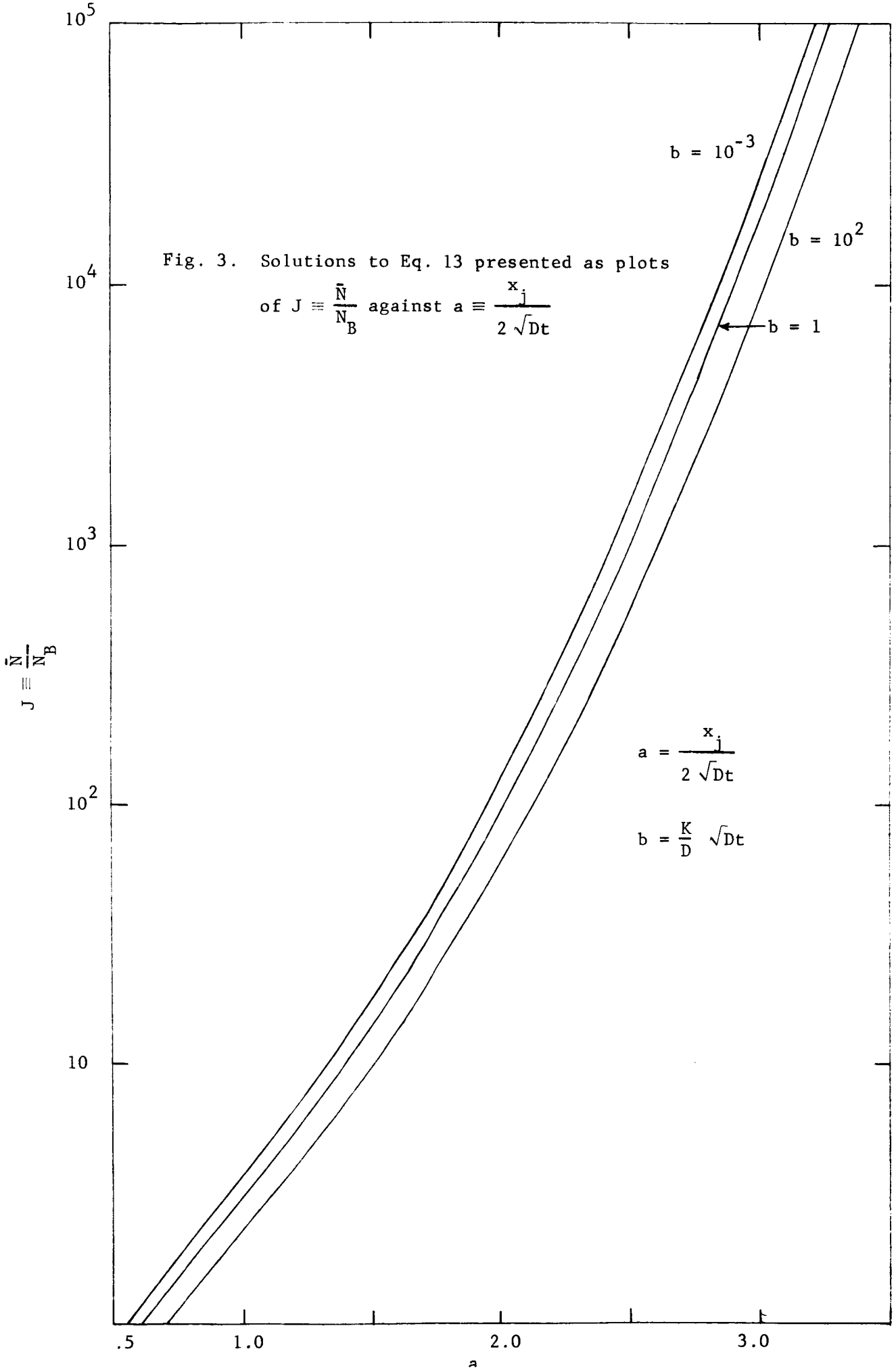

Fig. 3. Solutions to Eq. 13 presented as plots of $J \equiv \frac{\tilde{N}}{N_B}$ against $a \equiv \frac{x_j}{2\sqrt{Dt}}$

where

$$y_j = \frac{x_j}{2\sqrt{Dt}} \equiv a \quad ; \quad z = \frac{K}{D}\sqrt{Dt} \equiv b \ .$$

Plots of G as a function of a are shown in Fig. 2 on semi-log paper. The fact that these curves are nearly straight lines suggests that the exponential functional form is a good approximation of the relationship between G and a. Since the slope of the curves is negative, the general relationship may be written as:

$$G = G_o \, e^{-\alpha a} \tag{14}$$

where α is the slope of the straight line approximations to the curves in Fig. 2 and G_o, the a = 0 value of G.

Substituting Eq. 13 into Eq. 14,

$$\ln\left[\frac{N_B}{G_o N_{eq}}\right] = -\alpha a = -\alpha \frac{x_j}{2\sqrt{Dt}} \tag{15}$$

Rearranging the terms in Eq. 15 yields both

$$x_j = \frac{2\sqrt{Dt}}{\alpha} \ln\left[\frac{G_o N_{eq}}{N_B}\right] \tag{16}$$

and

$$a = \frac{1}{\alpha} \ln\left[\frac{G_o N_{eq}}{N_B}\right] \ . \tag{17}$$

The relationship between the diffusion coefficient and temperature T is empirically known to be expressible in an Arrenhius form [Ref. 2]:

$$D = D_o \, e^{-E_a/kT} \tag{18}$$

where E_a = an energy of activation,

D_o = a constant

k = Boltzman's constant.

The relationship between N_{eq} and the impurity concentration in the gas phase surrounding the silicon during diffusion is described by the partition coefficient k_g as follows [Ref. 4]:

$$N_{eq} = k_g c \tag{19}$$

Initially k_g will be assumed to be independent of c.

Substituting Eqs. 18 and 19 back into 16 results in the following explicit expression for x_j in terms of t, T, and c:

$$x_j = 2 \frac{\sqrt{D_o}}{\alpha} \sqrt{t}\, e^{-E_a/2kT} \left[\ln c - \ln \left(\frac{N_B}{G_o k_g} \right) \right] \tag{20}$$

Four constants $b_i (i = 0,1,2,3)$ are to be determined by fitting the data to the general model:

$$x_j = b_o\, t^{b_1}\, e^{-b_2/T} \left[\ln c - b_3 \right] , \tag{21}$$

where $b_o = 2 \frac{\sqrt{D_o}}{\alpha}$

$b_1 \simeq 0.5$

$b_2 = E_a/2k$

$b_3 = \ln \left[\frac{N_B}{k_g G_o} \right]$.

The constant b_2 so determined can be compared with the independently determined values of E_a, reported in the literature. The values of α and G_o cannot be estimated accurately from data plots similar to the theoretical plots shown in Fig. 2, since the slight errors introduced

by the exponential approximation can be magnified greatly outside of the appropriate range.

Neglecting any variation of mobility with concentration, the sheet resistivity ρ_s of a diffused layer is calculated from basic definitions as follows:

$$\bar{\sigma} = q\mu\bar{n} = \frac{1}{\rho_s x_j} \quad . \tag{22}$$

When all impurities are ionized, $\bar{n}$ in equation 22 is equal to $\bar{\eta}$, the average net impurity concentration. From Eq. 12,

$$\bar{\eta} = \bar{N} - N_B \quad . \tag{23}$$

Fig. 3 is a semi-logarithmic plot of $J \equiv \bar{N}/N_B$ as a function of a in which

$$\bar{N} = \frac{1}{a} \int_o^a N \, dy \tag{24}$$

and $a = \dfrac{x_j}{2\sqrt{Dt}}$ as before.

Over a limited range, the functional relationship is very closely exponential so that

$$\frac{\bar{N}}{N_B} = J_o \, e^{\beta a} \quad . \tag{25}$$

Substituting Eq. 25 back into Eq. 23 and then Eq. 22 yields

$$\rho_s = \frac{1}{q\mu x_j \bar{\eta}} = \frac{1}{q\mu x_j (N_B J_o e^{\beta a} - N_B) \, x} \quad . \tag{26}$$

Using Eq. 17 to eliminate a,

$$\rho_s = \frac{1}{q\mu x_j \, N_B \left(J_o \, e^{\frac{\beta}{\alpha} \ln \left[\frac{G_o N_{eq}}{N_B}\right]} - 1\right)} \tag{27}$$

which immediately yields

$$\rho_s = \frac{1}{q\mu x_j N_B \left(J_o \left[G_o \frac{N_{eq}}{N_B}\right]^{\beta/\alpha} - 1\right.} \tag{28}$$

Assuming $\beta/\alpha \approx 1$ and substituting for x_j from Eq. 21 and for N_{eq} from Eq. 19,

$$\rho_s = \frac{1}{q\mu \{b_o t^{b_1} e^{-b_2/T} [\ln c - b_3]\}(J_o G_o k_g c - N_B)}$$

$$= \frac{1}{b_o t^{b_1} e^{-b_2/T} [\ln c - b_3][b_4 c - b_5]}, \tag{29}$$

where b_o, b_1, b_2 and b_3 are the same as before (Eq. 21),

$b_4 = q\mu J_o G_o k_g$, and

$b_5 = q\mu N_B$.

Equation 29 is the model to be fitted to sheet resistivity data.

Information in the literature, based on empirical observations, suggests the following functional relationship between junction breakdown voltage $V_{(BR)}$ and the processing variables of diffusion [Ref. 5]:

$$V_{(BR)} \sim (Dt)^{k_1} . \tag{30}$$

Background concentration has been found to be extremely important but for the units examined here has been kept at a constant value of 2×10^{16} atoms/cm^3. Effects of surface concentration recently reported [Ref. 6] are ignored, at least initially, and the model form to be fitted is

$$V_{(BR)} = b_o \, t^{b_1} \exp\left(-\frac{b_2}{T}\right) \tag{31}$$

where $b_o \sim \sqrt{D_o}$

$b_1 = k_1$

$b_2 = E_a k_1 / 2k$, and

k_1 is arbitrary constant as suggested in Eq. 30.

The reverse current of a p-n junction can be divided into components according to the region in which they originate [Ref. 7]. Since both surface and space charge recombination-generation currents are thought to depend on variables not measurable in the present work (surface components depend on surface potential; space charge components, on trap sites), such current components are less attractive to model. Bulk diffusion currents, on the other hand, are simply calculated in terms of the available parameters. At room temperature they are extremely small in silicon but at elevated temperatures 150°C - 200°C, they increase rapidly and can dominate the observed current-voltage characteristics. The reverse current to be modeled will be assumed to be a diffusion current component and of the following form [Ref. 7]:

$$I_R = -\frac{kT_m}{q} \frac{b}{(1+b)^2} \sigma_i^2 \left(\frac{1}{\sigma_n L_p} + \frac{1}{\sigma_p L_n}\right) \tag{32}$$

where $b = \mu_n / \mu_p$

σ_i = intrinsic conductivity = $n_i q(\mu_n + \mu_p)$

σ_n = conductivity of n-region

σ_p = conductivity of p-region

L_p = diffusion length of a hole in n-region

L_n = diffusion length of an electron in p-region

T_m = temperature of measurement.

For a diffused layer the average conductivity can be substituted for σ_n and the functional form of the model becomes:

$$I_R = - \frac{kT_m}{q} \frac{b}{(1+b)^2} \sigma_i^2 \left(\frac{x_j \rho_s}{L_p} + \frac{1}{N_B q L_n} \right) . \qquad (33)$$

This equation is of the form:

$$I_R = b_o + b_1 (x_j \rho_s) , \qquad (34)$$

where $$b_o = - \frac{kT_m}{q} \frac{b}{(1+b)^2} \frac{\sigma_i^2}{N_B q \mu L_n}$$

$$b_1 = - \frac{kT_m}{q} \frac{b}{(1+b)^2} \frac{\sigma_i^2}{L_p}$$

3. Experimental Work

The experimental data for fitting the models of Sec. 2 were obtained with a diffusion system, employing phosphine gas as the original source of impurities [Ref. 1]. A schematic of the gas induction system is shown in Fig. 4. In such an arrangement, conventional gas metering equipment controls the flow rates of the various gases and permits control over the phosphine impurity concentration in the gas stream from about 0.01 ppm to 13,000 ppm. In all data reported here the total gas flow was 3000 cc/min; the oxygen concentration, 6700 ppm.

Two different furnace tubes were used. The first set of data employed GE 204 quartz shaped as follows:

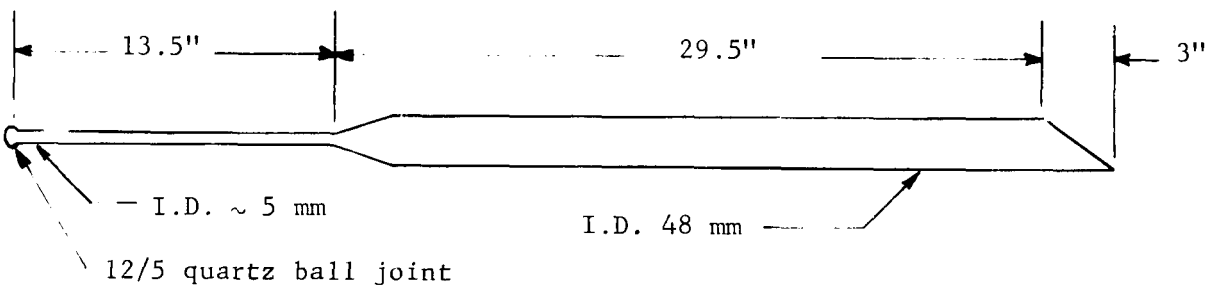

The tube was positioned in the furnace so that the joint between the large and the small bores was about 9 inches inside the furnace. The temperature at this point is typically within 100°C of the flat zone temperature. Quartz wool was packed around the small diameter tube to prevent excessive heat loss out the end of the furnace and to prevent the small diameter cantilevered section of the tube from sagging at high temperatures.

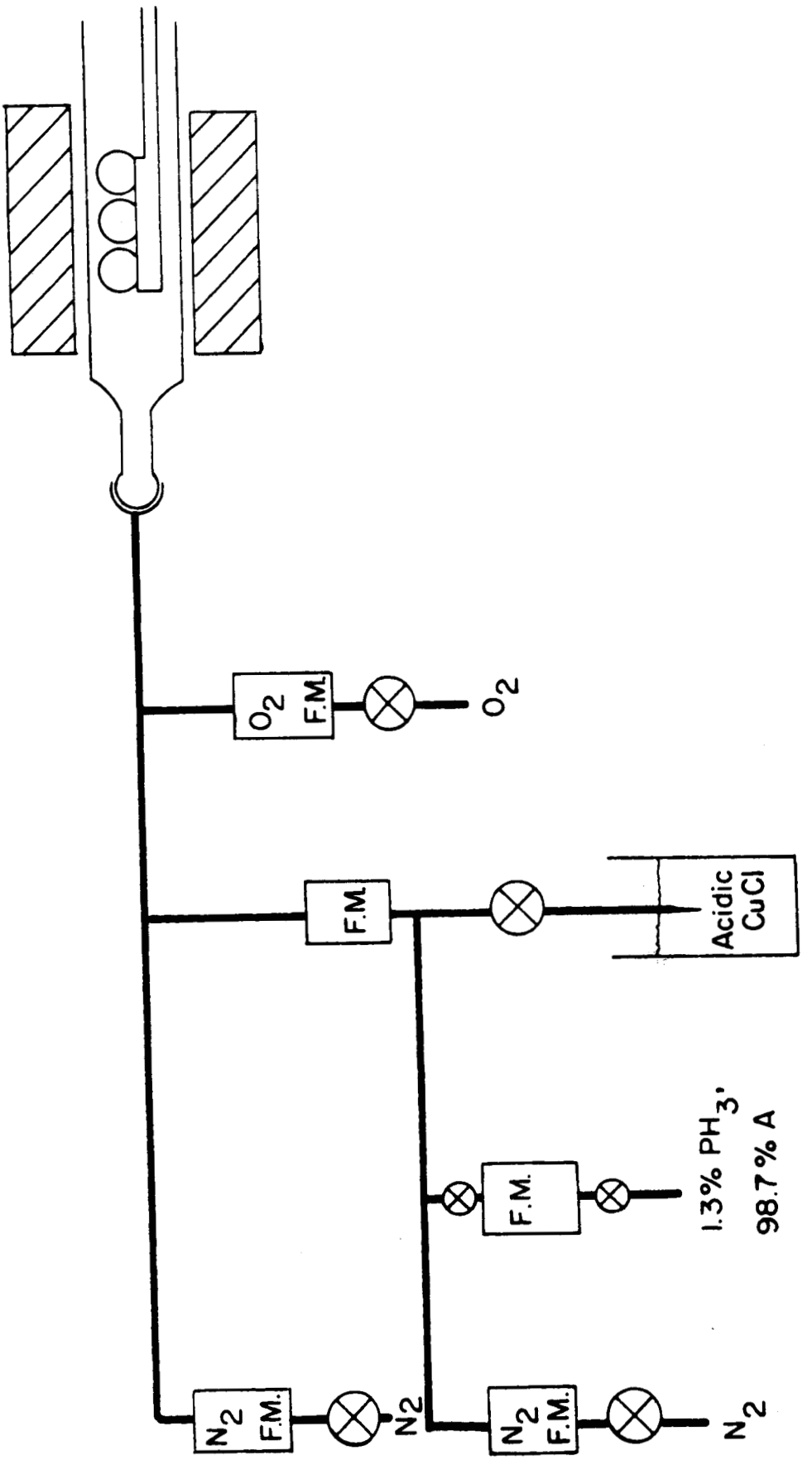

Fig. 4. Gas flow schematic for phosphine diffusion

The section of small diameter tubing is unusually long for two reasons:

1. It minimizes the back diffusion of P_2O_5 toward the room temperature portion of the system by maintaining a high velocity gas flow until the temperature of the tube walls is too high to gather any solid or liquid precipitate. No deposits of white, solid P_2O_5 are seen using this tube. With other tube geometries P_2O_5 can deposit at the neck between the high velocity and low velocity sections if the temperature at that point is not sufficiently high (> 500 - 600 °C).
2. The small diameter tubing over the region of maximum temperature gradient minimizes the bouyancy forces that have been shown to produce objectionable patterns of gas flow during diffusion [Ref. 8].

A second set of data was run using an AP 35 alumina (~99% Al_2O_3) tube, manufactured by the McDanel Refractory Porcelain Company to the following dimensions:

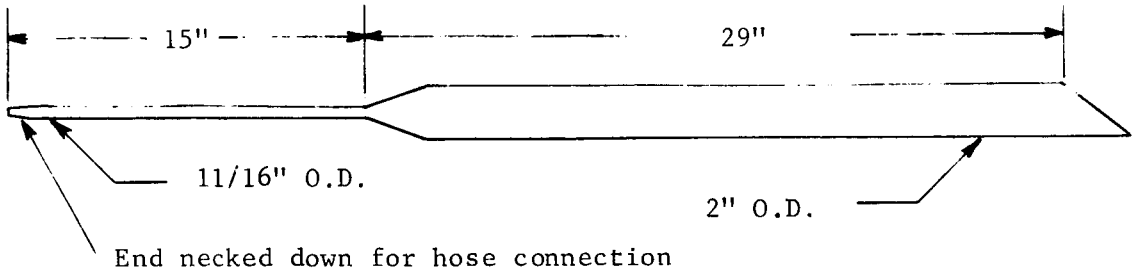

During all diffusions a single wafer was held vertically in a slotted boat made of the same material as the diffusion tube. The surface plane of the wafer was parallel to the direction of gas flow, the

wafer "standing" on its 1/4 inch orientation flat and the patterened side facing the right (as viewed from the open end of the furnace tube).

Twenty-seven points in t, T, c space were chosen for the initial factorial experiment:

t:	15	30	60	min
T:	1100	1150	1200	°C
c:	35	250	2450	ppm

The values of c are closer to the maximum value of c than they are to the minimum because:

1. This region is of most practical interest, i.e., 2450 ppm is suitable for forming the emitter of an n-p-n transistor; 35 ppm is perhaps appropriate for the base of an p-n-p transistor;
2. Reproducibility is better at the higher levels of impurity concentration;
3. The time of diffusion can be kept short; at lower impurity concentration, diffusion times in excess of one hour are necessary in order to obtain junctions deep enough to be evaluated accurately by the conventional junction depth and sheet resistivity methods.

The silicon used in these experiments was purchased from a commercial vendor to the following specifications:

Resistivity and Type: 1 ohm-cm $\pm$ 20% p-type

Growth Technique: Czrochralski

Orientation: <1 1 1> growth direction, 1/4 inch orientation flat cut parallel to the (1 1 0) plane

Dislocation Density: Etch pit count less than 5000 cm^{-2}

Dimensions: 0.75 - 0.90 inch diameter, 20 $\pm$ 2 mil thickness

Surface Finish: Both sides chemically polished

Wafer preparation, prior to its arrival at our laboratory, consisted of sawing the ingot into slices 26-mil thick, lapping to about 23 mils, and etching (chemical polishing) to the final dimension of 20 mils. No checks other than visual inspection were performed to assure that all mechanical damage was removed by this process.

Upon receipt by our laboratory, the incoming wafers were classified according to resistivity into the following groups:

No. of Wafers	Resistivity Spread (ohm-cm)	Background Impurity Doping (cm^{-3})
15	less than 0.80	$\times 10^{15}$
105	0.80 - 0.89	7×10^{15}
80	0.90 - 1.04	6×10^{15}
5	1.05 - 1.20	5×10^{15}

Only wafers from the most populous group (0.80 - 0.89 Ω-cm) were used in the diffusion experiments.

Photoengraving masks were designed to allow a single diffusion to furnish data for modeling both the intermediate-diffusion process-parameters, x_j and ρ_s, and the electrical device properties I_R and $V_{(BR)}$. Figure 5 is a photograph of the glass mask actually used to expose photoresist prior to etching for diffusion. The dark areas in the photograph represent the areas into which impurity diffusion takes place.

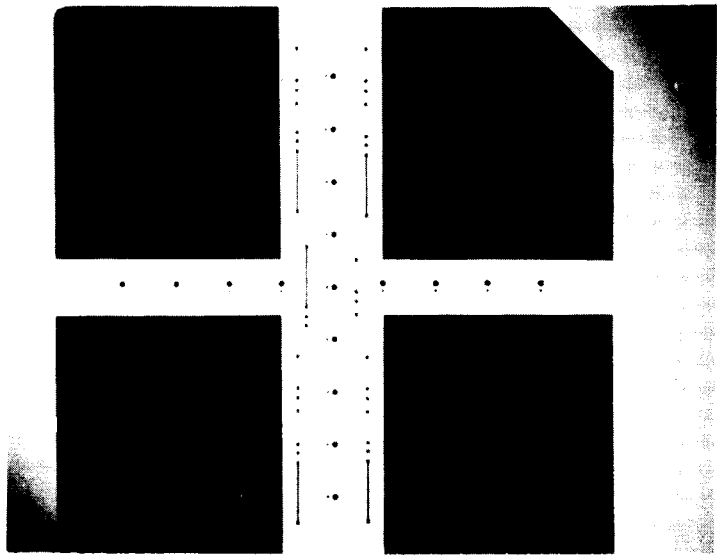

a. Overall view

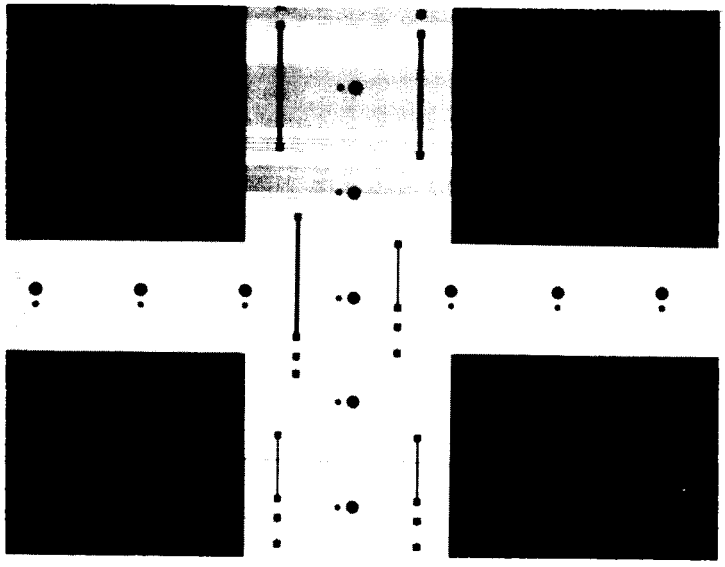

b. Enlargement of center section

Fig. 5. Photomask for defining areas of diffusion

The light areas correspond to regions that are covered with oxide during the diffusion step. The circular areas define diode pairs, whose diameter is either 4.5 mils or 9 mils. Consequently the perimeter of the larger planar diode is twice that of the smaller, while its area is four times as large. These diode pairs are arranged in a cross, consisting of four arms radiating from the center. The radial distance of corresponding diode pairs is the same in each arm. Seventeen diode positions are included, four each centered about a radius of 0.075N inch where N = 1,2,3,4 and then one at the center of the wafer.

In addition to the diode positions, several resistors are included along the sides of the horizontal diode arms. Resistors of 25 squares of diffused area appear 20 times. Four different widths are repeated five times each--0.4, 0.8, 2.0, 3.5 mils. For all resistors the length/width ratio is the same so that the absolute value of these resistors should be the same to first order. In addition to providing an independent check of the sheet resistivity of the diffused layer, the observed variation in resistor value should indicate any dependence of this value on dimensions as well as any differences in spreads of values with dimensions.

Contacts to the diffused regions were defined by the mask pictured in Figure 6. The dark regions correspond to regions on the wafer to which ohmic contact was made.

Operating Procedures

The wafers used in the experiment were processed according to the following specifications:

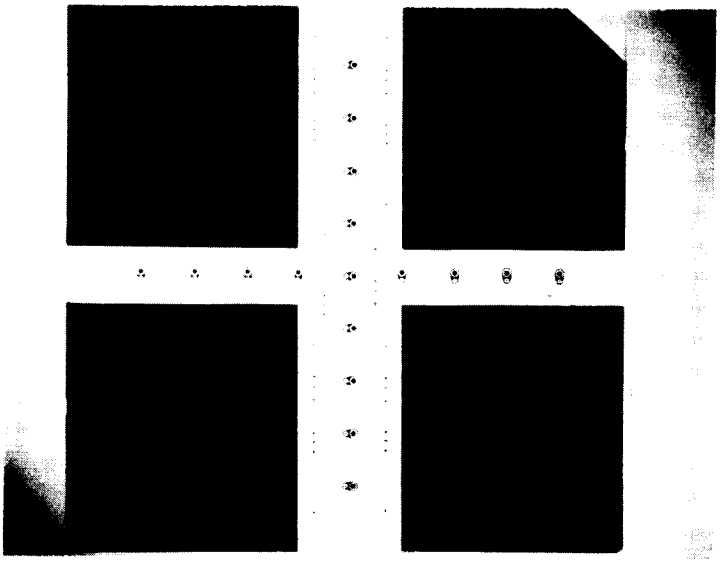

a. Overall view

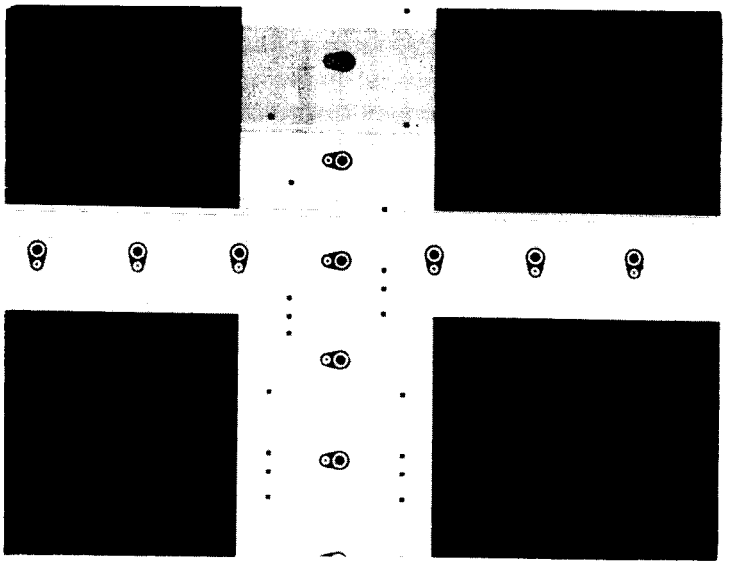

b. Enlargement of center section

Fig. 6. Photomask for defining areas of ohmic contact

1. Clean all wafers chemically and oxidize in steam to an oxide thickness of about 5500 A.
2. Coat all wafers immediately with 1:1 mixture of KTFR (Kodak Thin Film Resist) and KMER thinner and store in a clean, dark place.
3. As required print one wafer with mask No. 1 (Fig. 5) and etch.
4. Remove photoresist, clean, and diffuse as programmed.
5. Following diffusion, immerse the entire wafer in buffered HF etch for 1 minute.
6. Make 8 four point probe resistivity measurements on each side of the wafer as shown below:

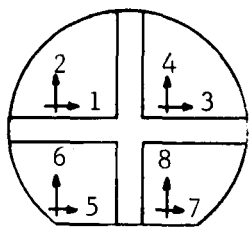

7. Groove both sides of the wafer in each quadrant for junction depth measurements.
8. Delineate junctions, measure junction depth and reoxidize wafer.
9. Coat wafer immediately with photoresist and store until ready to make ohmic contacts.
10. Align and print mask No. 2 (Fig. 6) for etching ohmic contact windows.
11. Etch and immediately evaporate 1000 A of aluminum over the entire wafer.

12. Remove photoresist (and aluminum deposited thereon) by ultrasonic agitation in trichlorethylene and gentle swabbing. (Figs. 7 and 8 are photomicrographs of a wafer after this step in the processing.)
13. Store wafer in dessicator until ready to measure electrical properties.
14. Place wafer on hot plate whose surface is 200°C.
15. Using anodized tungsten probes make pressure contacts to the appropriate sides of the diodes and cover wafer with a metallic canopy.
16. Measure reverse current at V_R = 1, 5, 10, 20, 50 vdc.
17. Measure reverse voltage at I_R = 200, 300, 400 μA.

All the preceding steps were accomplished using "standard" techniques as described in Silicon Integrated Device Technology, Vols. III, IV, and VII [Refs. 2, 9, 10]. Special practices peculiar to this diffusion technique were:

1. The wafers were loaded into the furnace and permitted to come up to equilibrium for 5 mins. prior to starting the impurity gas flow.
2. Prior to each run at an impurity concentration different from that previously run or prior to the first run of the day, a dummy run was performed in which the impurity flow was turned on to establish the new desired concentration level but no wafer was loaded. This run was for 30 min. and 10 - 20 min. following this dry run, the actual diffusion was begun. For subsequent diffusions at the same concentration but different

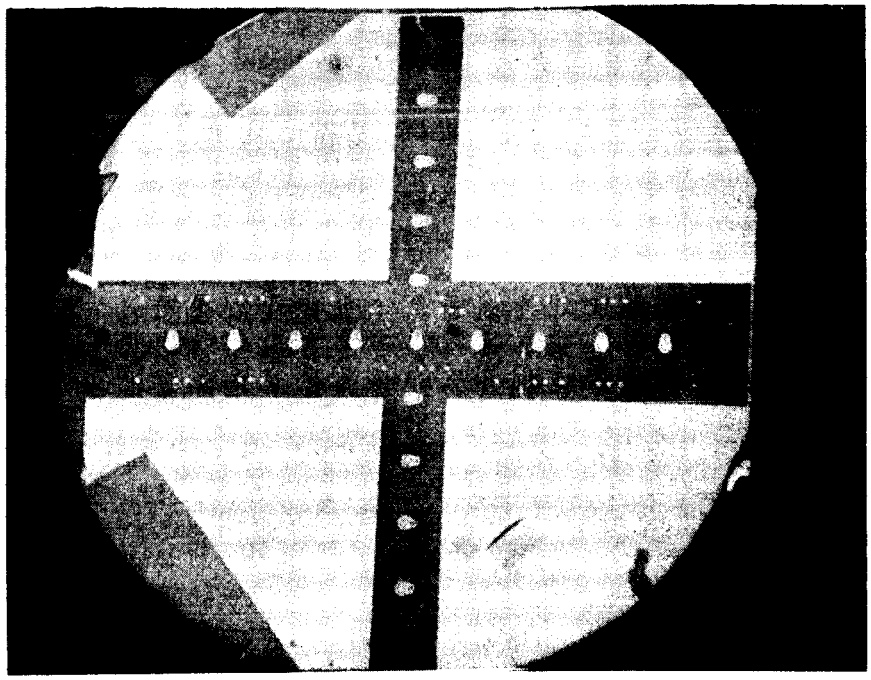

a. Overall view

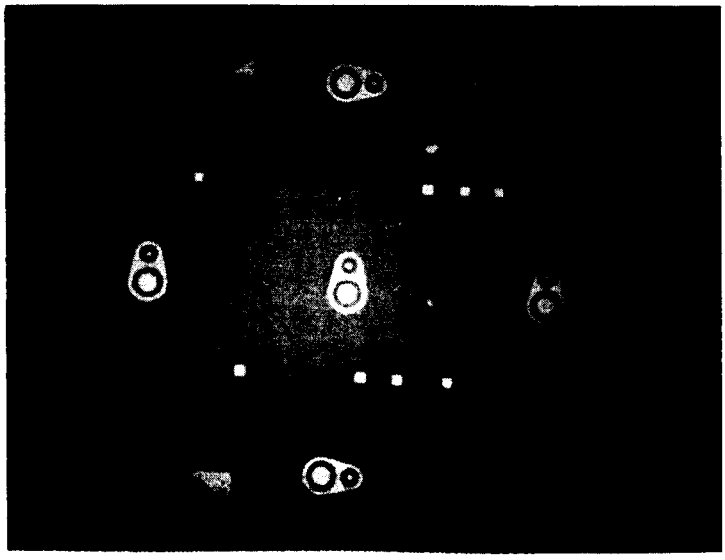

b. Enlargement of center section

Fig. 7. Wafer following processing

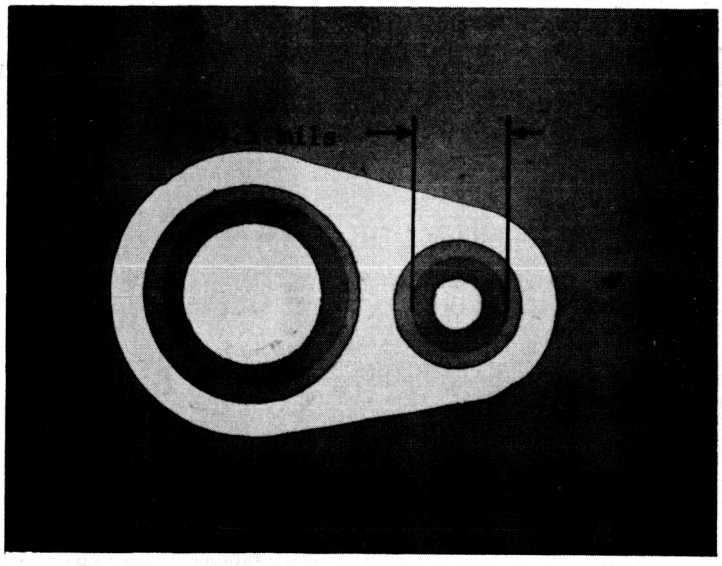

a. Diode position

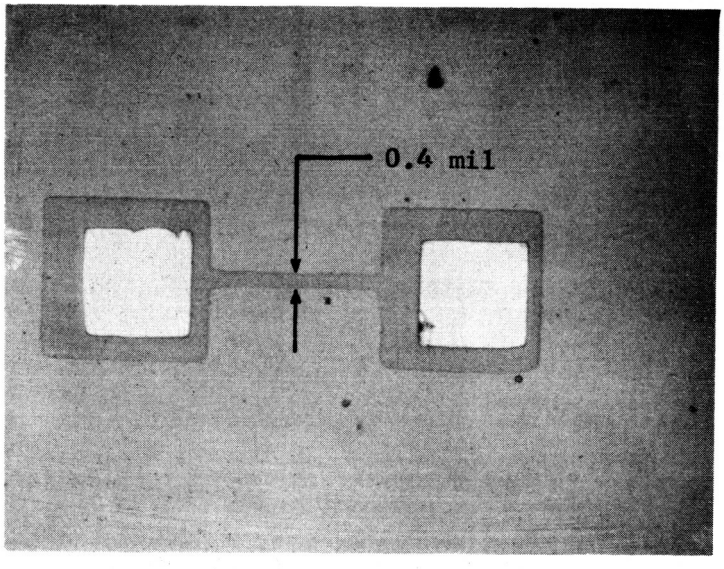

b. Resistor

Fig. 8. Photomicrograph of units on a completed wafer

times no dummy run was made since the losses to the system walls were expected to be balanced by the gains, i.e., there would be no net change in impurity concentration due to background effects.

3. All wafers were loaded and unloaded rapidly--no attempt was made to preserve lifetime by slow cooling.
4. The load during all diffusions consisted of one whole wafer only.
5. Nitric acid was the last acid used on the surface prior to diffusion, guaranteeing a thinly oxidized surface as the initial surface for diffusion.

Figures 7 and 8 show portions of a processed wafer ready for electrical test. Figure 7a is a photomicrograph of the whole wafer and Figs 7b, 8a and 8b are blowups of various sub-sections of that wafer. Figure 7b is the center section; Figs. 8a and 8b show a diode pair and the smallest resistor (width = 0.4 mils, length = 10 mils, no. of squares = 25), respectively. In all photos the aluminum deposits appear white; and the n-type diffused regions are slightly darker than the surrounding substrate surface. Grooves for measuring junction depth are marginally visible in each of the quadrants of the wafer pictured in Fig. 7a.

Sheet resistivity measurements were read directly from the scale of a Texas Instruments' rho-meter, Model 235B. This meter has five probes, four of which are equally spaced in a line to form the conventional four point probe arrangement. The fifth is somewhat removed from the four and permits a large dc bias to be placed between the four

measuring probes and this fifth, biasing probe. The resistivity is measured by a superimposed ac current and voltage; the meter reads directly in ohms/square.

Junction depth measurements were made by counting interference fringes formed by reflection of a monochromatic beam from a grooved surface [Ref. 11]. A commercial wafer sectioning machine--Model 310 by Micro Tech Inc., Sunnyvale, California--was used to form the cylindrical grooves. Typically four separate measurements of junction depth were made on each side of a diffused wafer--one in each quadrant. Junction delineation was accomplished by use of an HF type solution (most often commercial 46% HF) flooded with light from a microscope illuminator.

The measurement of reverse current I_R and breakdown voltage V_{BR}, came from the circuit sketched in Fig. 9.

The initial check, after making point contacts to a diode, was to observe the junction I-V characteristics on a curve tracer. If the reverse current was large enough to be measured by the scales on the curve tracer, the values of current at reverse voltages of 1, 5, 10, and 20 were recorded. For all diodes the voltage at a reverse current of 200, 300, and 400 μ A were recorded. The reverse current of high quality, "good" diodes could not be read in this manner and a separate dc power supply and voltmeter were employed to measure all currents under 10 μ A. As indicated in Fig. 9, the dc voltmeter was first used to adjust the output of the power supply to the desired voltage and then was used, by switch B, to measure the voltage drop across a precision

resistor of 10^5 ohms. This reading immediately yielded the value of reverse current.

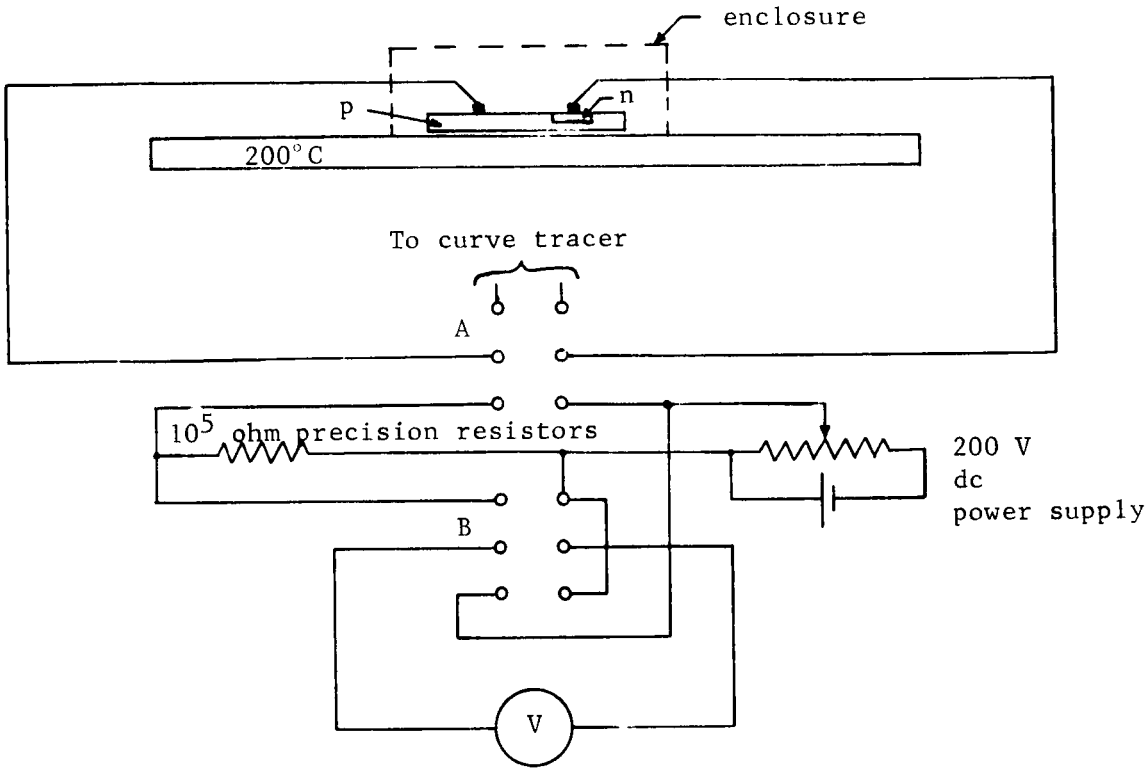

Fig. 9. Schematic of measuring circuit for diode electrical properties

4. Data Evaluation

Raw data from the first factorial experiment, using the silicon wafers described in Sec. 3, are listed in Table 1. The final equations obtained by a least squares fit of the models given in Sec. 2 are:

$$\hat{x}_j = 1.364 \times 10^7 \; t^{0.66} \; e^{-\frac{14750}{T}} \; (\ln c - 0.52) \; A \qquad (35)$$

$$R = 0.97 \qquad s(x_j) = 2900$$

$$\hat{\rho}_s = \frac{1.647 \times 10^4 \; t^{-1.4} \; e^{\frac{5000}{T}}}{c(\ln c - 0.5)} \; \text{ohms/}\square \qquad (36)$$

$$R \simeq 0.90 \qquad s(\rho_s) = 15.1$$

$$\ln \hat{V}_{(BR)} = 5.005 + 0.072 \ln t - \frac{2084}{T} \; \text{volts} \qquad (37)$$

$$R = 0.68 \qquad s(\ln V_B) = 0.073$$

$$\hat{I}_{R_{(L)}} = 9.27 + 0.21 \; x_j \rho_s \; \mu A \qquad (38)$$

$$R = 0.47 \qquad s(I_{R_{(L)}}) = 8.77$$

$$\hat{I}_{R_{(S)}} = 4.85 + 0.100 \; x_j \rho_s \; \mu A \qquad (39)$$

$$R = 0.44 \qquad s(I_{R_{(S)}}) = 4.60$$

R is the multiple correlation coefficient defined as:

$$1 - R^2 = \frac{\Sigma(\text{measured values - calculated values})^2}{\Sigma(\text{measured value - median measured value})^2} \; . \qquad (40)$$

Table 1

Raw Data from First Diffusion Experiment

1 Ω cm p-type Substrate

(1) Wafer No.	(2) Temp. (°C)	(3) Concentration (ppm)	(4) Time (minutes)	(5) ρ_s (Ω/□) Top (Averages)	(6) ρ_s (Ω/□) Bot (Averages)	(7) ρ_s (Ω/□) Top (Medians)	(8) ρ_s (Ω/□) Bot (Medians)	(9) x_j (A) Top	(10) x_j (A) Bot	(11) $\rho_s x_j$ Top (10^{-4} ohm-cm)	(12) $\rho_s x_j$ Bot (10^{-4} ohm-cm)	(13) $V_{(BR)}$ 200°C	(14) I_R (μA) L	(15) I_R (μA) S
A-38	1100	35	15	139	128	120	130					35	15	7.5
A-53	1100	35	30	16.5	13.8	16.65	13.85	10160	10160	16.8	14.0	37	8.5	4.0
A-7	1100	35	60	10.8	8.72	11	8.5	12700	12700	13.7	11.0	40		
A-61	1100	35	120	11	11	11.75	11	17800	19000	19.6	20.9	47	20	10
A-21	1100	250	15	11.27	10.45	11	10.7	7620	10080	8.6	10.05	42	7.0	3.0
A-45	1100	250	30	3.94	3.33	.385	3.35	15300	17800	6.0	5.93	44	1.0	6.0
A-25	1100	250	60	3	2.53	3	2.5	28000	29200	8.4	7.40	46	3.5	2.5
A-17	1100	2450	15	5.2	3.66	5.1	3.7	10080	12700	5.25	4.65	35	9.0	3.0
A-35	1100	2450	30	3.25	2.18	3.15	2.2	20400	20400	6.62	4.45	46	2.0	1.0
A-39	1100	2450	60	1.96	1.4	1.95	1.41	30500	30500	5.98	4.27			
A-49	1150	35	15	170	178	177	175	5080	5080	86.4	90.5	43	18	7.0
A-11	1150	35	30	52.5	55	53	54	12900	12900	67.6	70.9			
*A-31	1150	35	30	41	27.6	40	27.25	12700	12700	52.1	35			
A-3	1150	35	60	19	17	18	16.75	20320	20320	38.6	34.6	45	27	14
A-4	1150	35	120	8.36	5.74	8.25	5.8	33000	40600	27.6	23.3	48	22	11
A-24	1150	250	15	6.23	5.4	6.3	5.4	17800	17800	11.1	9.6	46		
A-33	1150	250	30	3.45	2.9	3.42	2.95	24100	25400	8.32	7.4	43	18	12
A-46	1150	250	60	2.35	2	2.32	2	38200	38200	9.0	7.6	51	12	6.0
A-16	1150	2450	15	3.07	2.25	3	2.27	19000	19000	5.8	4.3	39	4.0	2.0
A-18	1150	2450	30	2.35	1.725	2.2	1.72	29200	29200	6.8	5.0	44	10	5.0
A-22	1150	2450	60	1.44	1.1	1.42	1.1	40600	40600	5.85	4.47	49	8.0	4.0
A-43	1200	35	15	60	44.5	58.5	44	10160	11400	60.4	50.7	44	15	10
A-20	1200	35	30	34.5	30	33.75	30	15250	15250	52.5	45.7	47		
A-36	1200	35	60	19.4	16.1	19.5	15	25400	25400	49.3	40.9	48	40	20
A-1	1200	250	15	6.6	5.4	6.55	5.35	20300	20300	13.6	11.0	50	20	12
A-12	1200	250	30	4.8	3.83	4.7	3.8	30500	35600	14.6	13.6	44	11	5.0
A-42	1200	250	60	3.14	2.41	3.1	2.4	45600	48400	14.3	11.7	43	30	15
A-13	1200	2450	15	2.31	1.85	2.3	1.8	25400	30500	5.9	5.64	44	1.6	0.8
A-19	1200	2450	30	1.48	1.22	1.45	1.22	40600	35600	6.0	4.35			
A-15	1200	2450	60	.962	.8	.95	.8	66200	21000	6.3	4.86			

NOTE: * A-31 followed A-4 by 10 min

The standard deviation, s, is defined by

$$s^2 = \frac{\Sigma(\text{measured value - calculated value})^2}{\text{no. of observations - no. of parameters evaluated}} \qquad (41)$$

The practical significance of these statistical definitions is that the standard deviation gives the uncertainty to be expected in this process. Specifically, for a Normal (Gaussian) distribution* 68% of the measured values of x_j are expected to be in the range $\hat{x}_j \pm s$; 95%, in the range $\hat{x}_j \pm 2s$. R^2 is the proportion of the variance of the measured values which is explained by the model. Values of R close to unity plus values of s less than about 10% of the total span of the measured variable are reasonable criteria for determining when the model and the process are adequate (at least for interpolation). The models for $\hat{x}_j$ and $\hat{\rho}_s$ are close to "adequate" by these criteria. The models for $V_{(BR)}$ and I_R are not.

Equation (35) is plotted in Figs. 10 - 12, showing the relationships between junction depth and impurity concentration (Fig. 10), temperature (Fig. 11), and time (Fig. 12). Residuals--the difference between the expected value of x_j as calculated from Eq. 35 and that actually measured--are plotted in Fig. 13. The points representing the residuals are fairly randomly distributed about the zero residual axis, indicating the model is not particularly biased toward certain ranges of x_j and that the model seems equally applicable for both large and small values of junction depths.

---

* This is true if the degrees of freedom (denominator in Eq. 41) is quite large. If not, the fraction is reduced and depends upon the degrees of freedom according to the "students" t distribution.

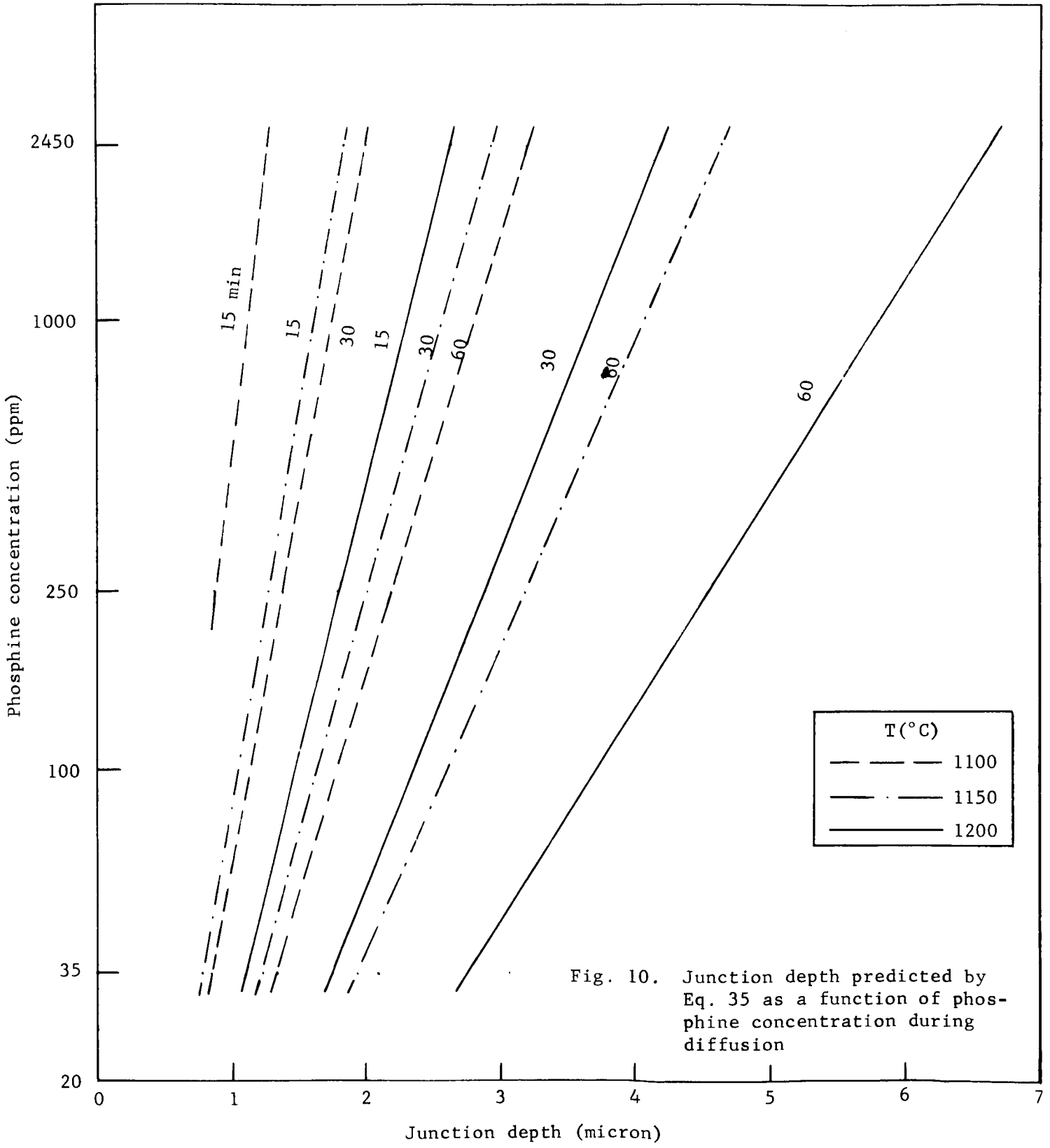

Fig. 10. Junction depth predicted by Eq. 35 as a function of phosphine concentration during diffusion

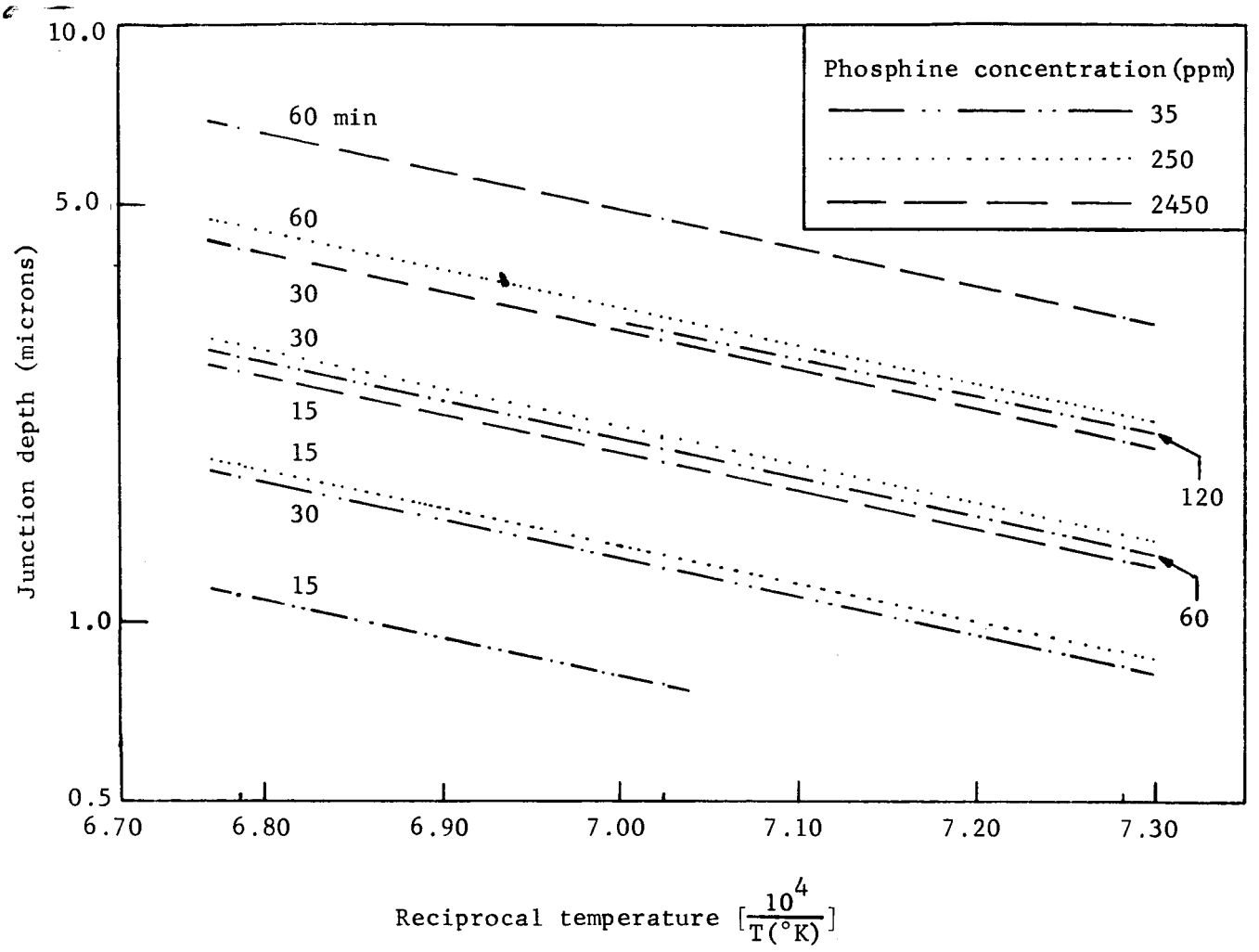

Fig. 11. Junction depth predicted by Eq. 35 as a function of diffusion temperature

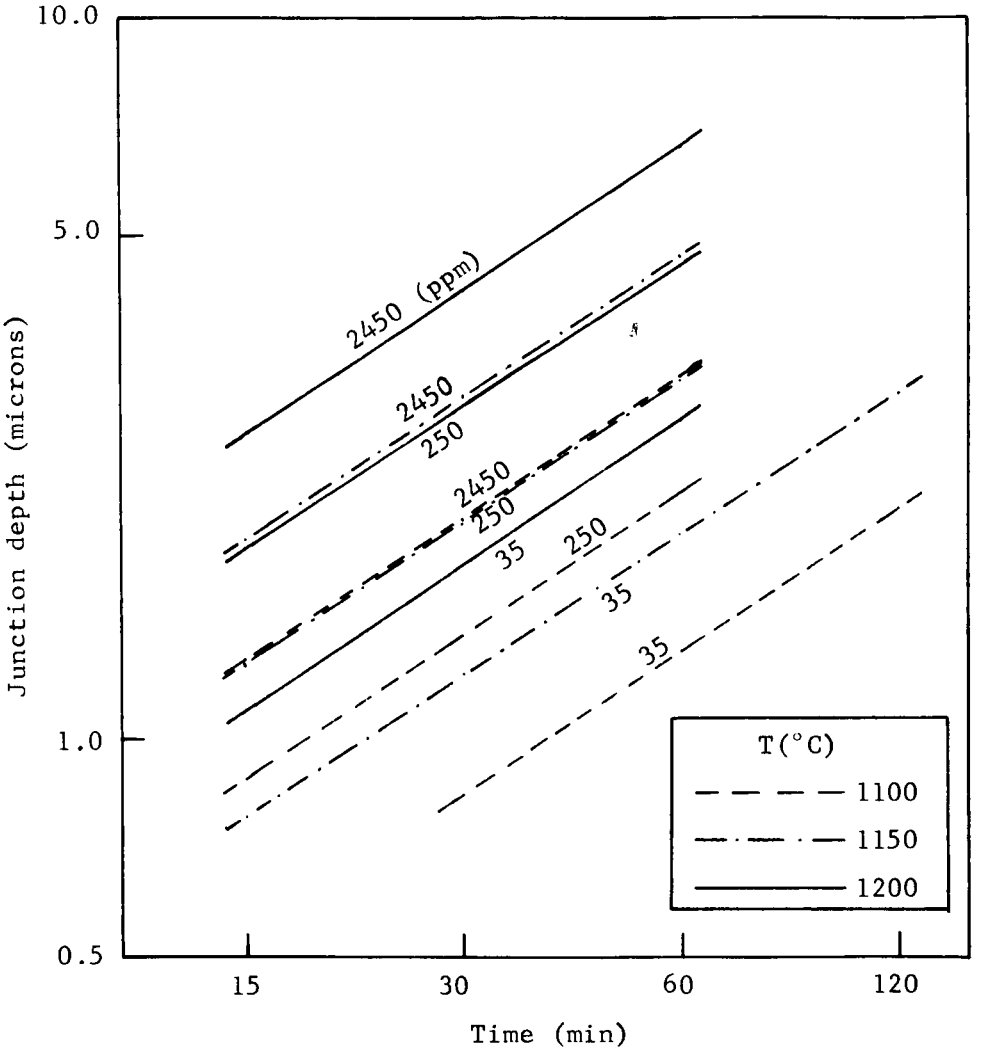

Fig. 12. Junction depth predicted by Eq. 35 as a function of diffusion time

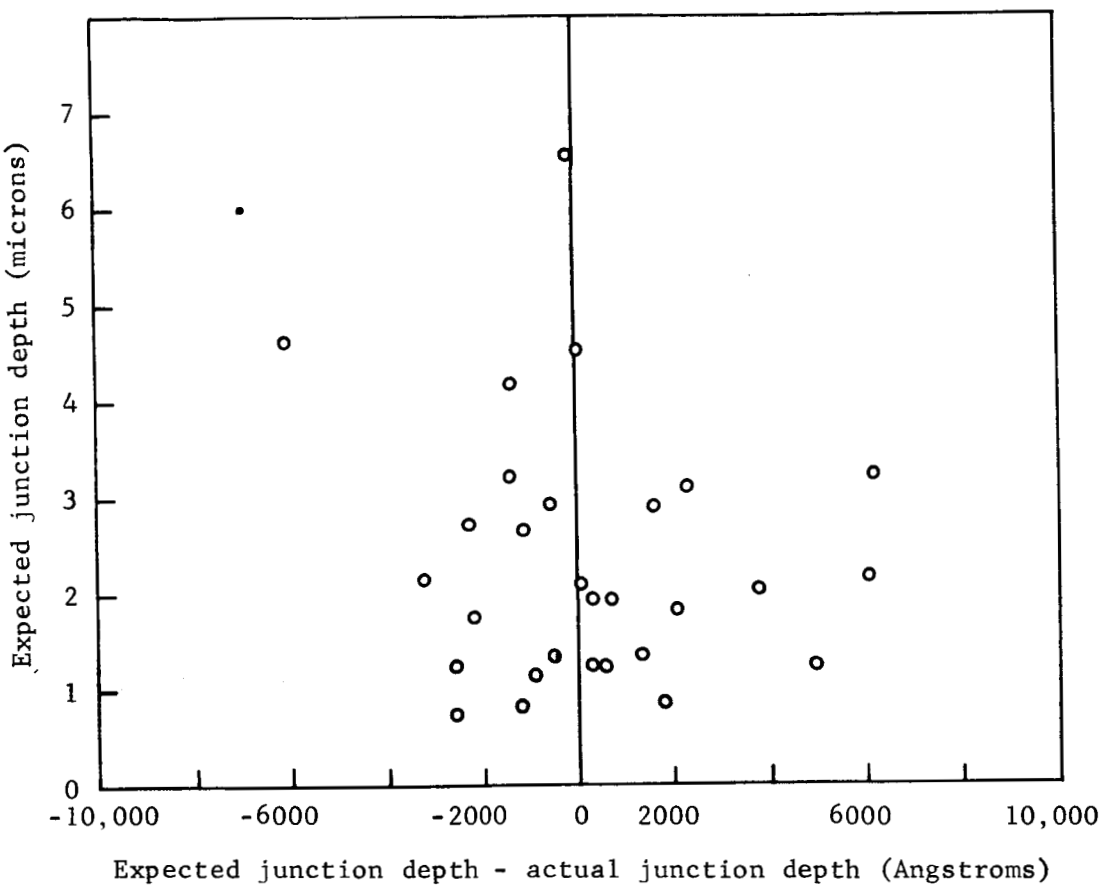

Fig. 13. Distribution of residuals from Eq. 35 and the top surface data of Table 1

The value of the coefficient b_2 (Eqs. 21 and 35) can be used to determine the activation energy of the diffusion process. From the coefficient fitted in Eq. 35, the following value of E_a is derived:

$$E_a = (2k)(14750°K)$$

$$E_a = 2\left(\frac{8.63 \times 10^{-5} \text{ e.v.}}{°K}\right)(14650°K)$$

$$\approx 2.50 \text{ e.v.} \qquad (42)$$

Values for E_a of 2.4 to 3.7 e.v. appear in the literature, depending upon the surface concentration of the diffusing impurity and the substrate doping level [Ref. 3].

In Table 2, measured values of ρ_s are compared with the values calculated from Eq. 36. The standard deviation is greater than the magnitude of many of the measured values themselves. The three checked points in Table 2, having by far the largest residuals, are responsible for the size of the standard deviation. These points represent the minimum time and minimum concentration diffusions at each temperature. Their elimination would reduce the magnitude of s considerably.

The functional form of Eq. 36 does not adequately predict the observed temperature dependence of sheet resistivity for the two lower values of impurity concentration in the gas flow (35 ppm and 250 ppm). Figure 14 compares the shape of the curve predicted by Eq. 36 with that of the observed curves at both 35 and 250 ppm. The observed data clearly indicates a departure from the simple exponential temperature dependence assumed. At the highest values of impurity concentration (c = 2450 ppm),

Table 2

Residuals Calculated from the Observed Sheet Resistivity
(Aveg. Top Surface Data, Table 1) and the Predicted (Eq. 36)

T	C	t	ρ_s, Top, Meas.	ρ_s, Top, Calc.	ρ_s(Meas.) - ρ_s(Calc.)	
1100	35	30	16.5000	50.2373	-33.7373	✓
		60	10.8000	19.0364	- 8.2364	
		120	11.0000	7.2134	3.7866	
	250	15	11.2700	11.2935	- 0.02346	
		30	3.9400	4.2794	- 0.3394	
		60	3.0000	1.6216	1.3784	
	2400	15	5.2000	0.7923	4.4077	
		30	3.2500	0.3002	2.9498	
		60	1.9600	0.1138	1.8462	
1150	35	15	170.0000	116.6533	53.3467	✓
		30	52.5000	44.2034	8.2966	
		30	41.0000	44.2034	- 3.2034	
		60	19.0000	16.7499	2.2501	
		120	8.3600	6.3470	2.0130	
	250	15	6.2300	9.9370	- 3.7070	
		30	3.4500	3.7654	- 0.3154	
		60	2.3500	1.4268	0.9232	
	2450	15	3.0700	0.6971	2.3729	
		30	2.3500	0.2642	2.0858	
		60	1.4400	0.1001	1.3399	
1200	35	15	60.0000	103.5378	-43.5378	✓
		30	34.5000	39.2335	- 4.7335	
		60	19.4000	14.8667	4.5333	
	250	15	6.6000	8.8198	- 2.2198	
		30	4.8000	3.3421	1.4579	
		60	3.1400	1.2664	1.8736	
	2450	15	2.3100	0.6187	1.6913	
		30	1.4800	0.2345	1.2455	
		60	0.9620	0.08884	0.8732	

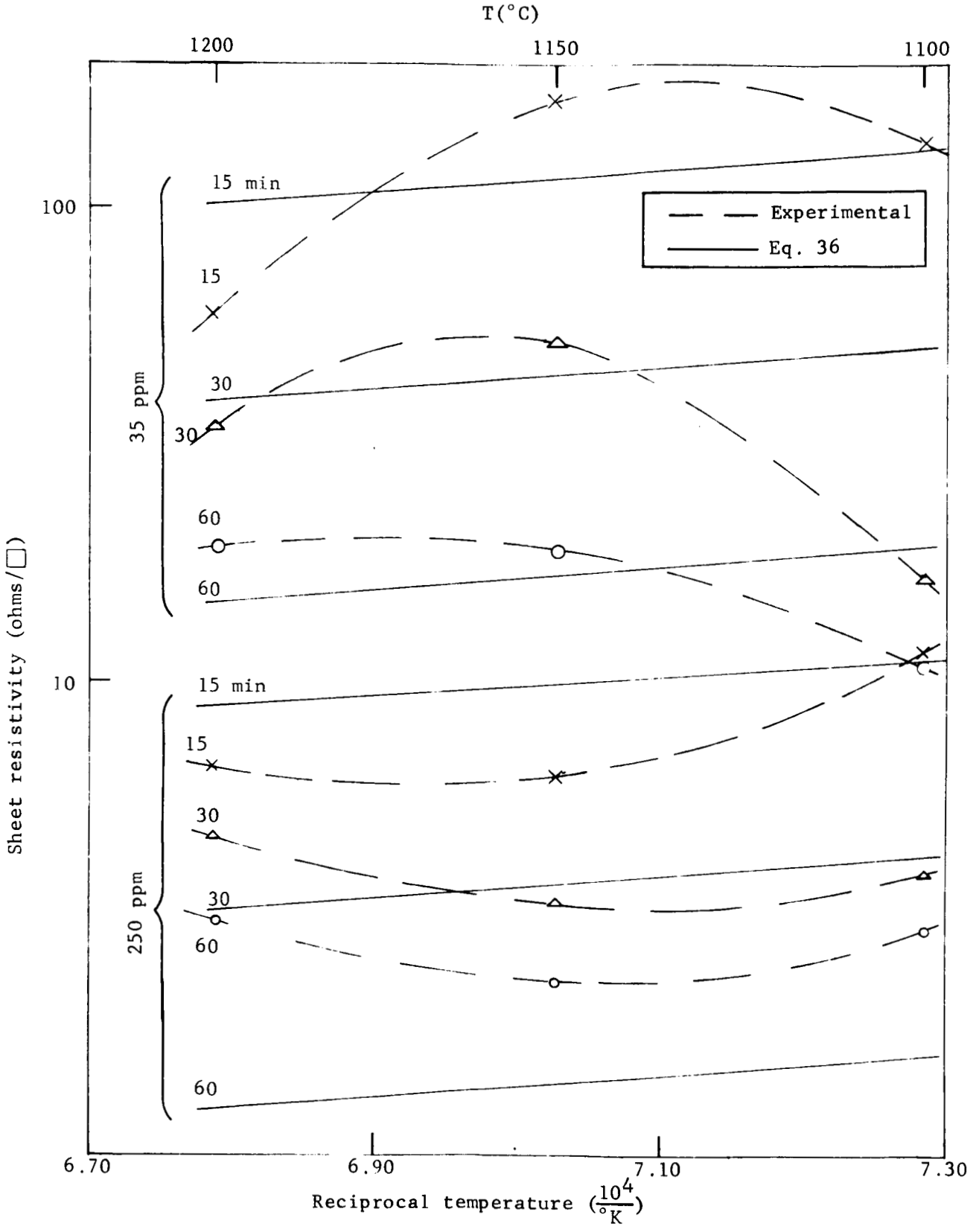

Fig. 14. A comparison of sheet resistivity as predicted by Eq. 36 and that observed (aveg. top surface data, Table 1) for the lower values of impurity concentration

however, such an exponential temperature dependence is observed, as shown in Fig. 15. Figure 15 is the same plot as Fig. 14 except that the low concentration data have been replaced by higher concentration data. The exponential functional form predicted seems to be very reasonable here since both the predicted and observed curves are straight lines in this semi-logarithmic plot. The slopes and intercepts of the predicted curve differ from those observed but, as is evident in Table 2, a few low c points are exercising undue influence in the least squares fit of these parameters. The least squares fit yields the values that result in minimum total residual over the entire range of the variables investigated. If the lower two values of c are eliminated from the curve fitting, and the model is fitted only to the c = 2450 data, the following relationship results:

$$\hat{\rho}_s = 0.03587\ t^{-0.77}\ e^{\frac{14,000}{T}}$$

$$R \simeq 0.97 \qquad s(\rho_s) = 0.26 \qquad (43)$$

Equation 43 is plotted in Fig. 16 along with the experimental points on which the equation is based. Over this extremely limited range of values, this model appears quite adequate for purposes of practical fabrication.

To include lower values of c (and hence obtain higher values of ρ_s) alterations in the form of Eq. 36 are needed. These alterations would be of significance only for values of c less than 2450. At $c \approx 2450$, the model would be similar to that expressed in Eq. 43.

A tentative conclusion of observations just stated is that the exponential approximation to the exact solutions of the diffusion

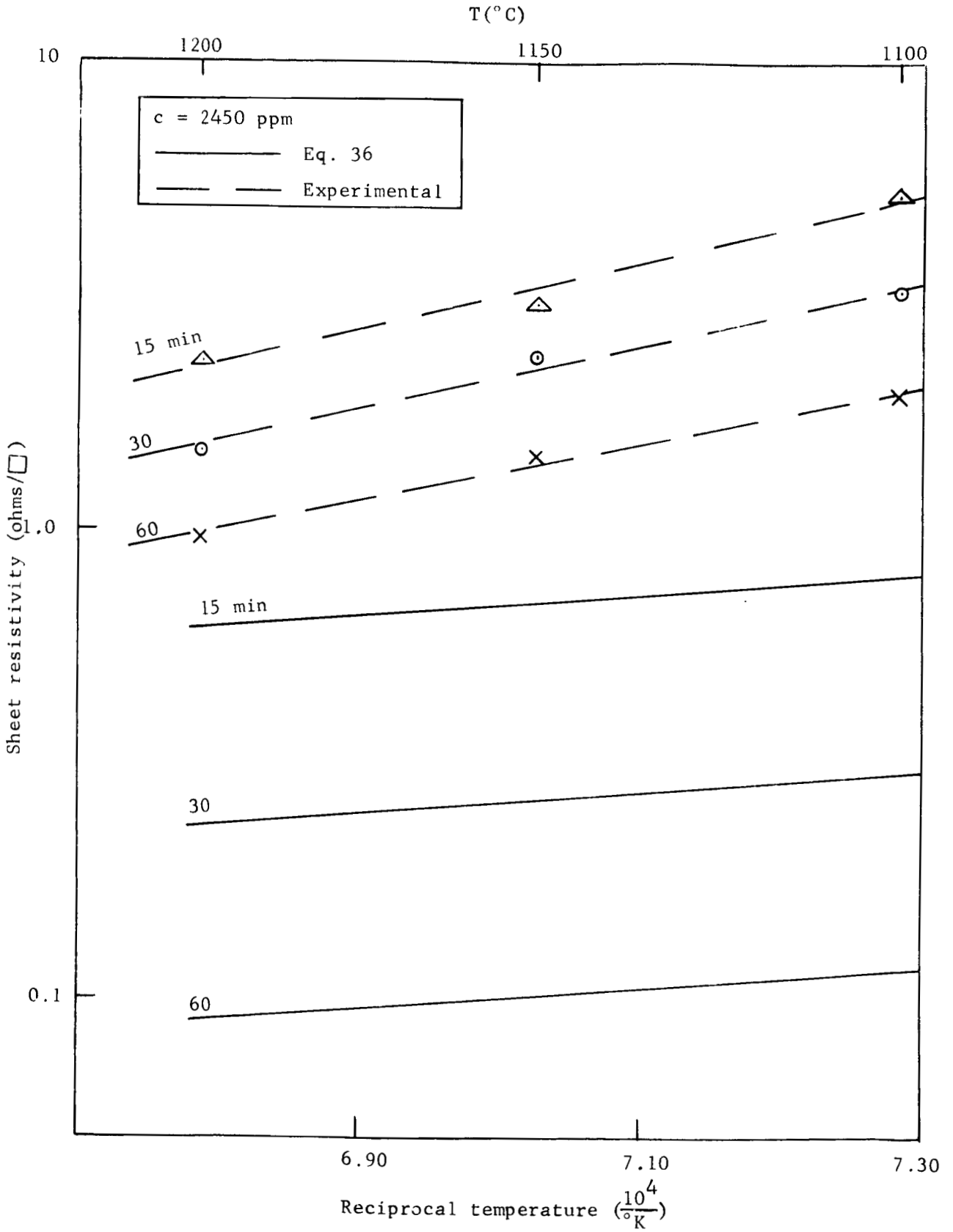

Fig. 15. A comparison of sheet resistivity as predicted by Eq. 36 and that observed (aveg. top surface data, Table 1) for the highest value of impurity concentration

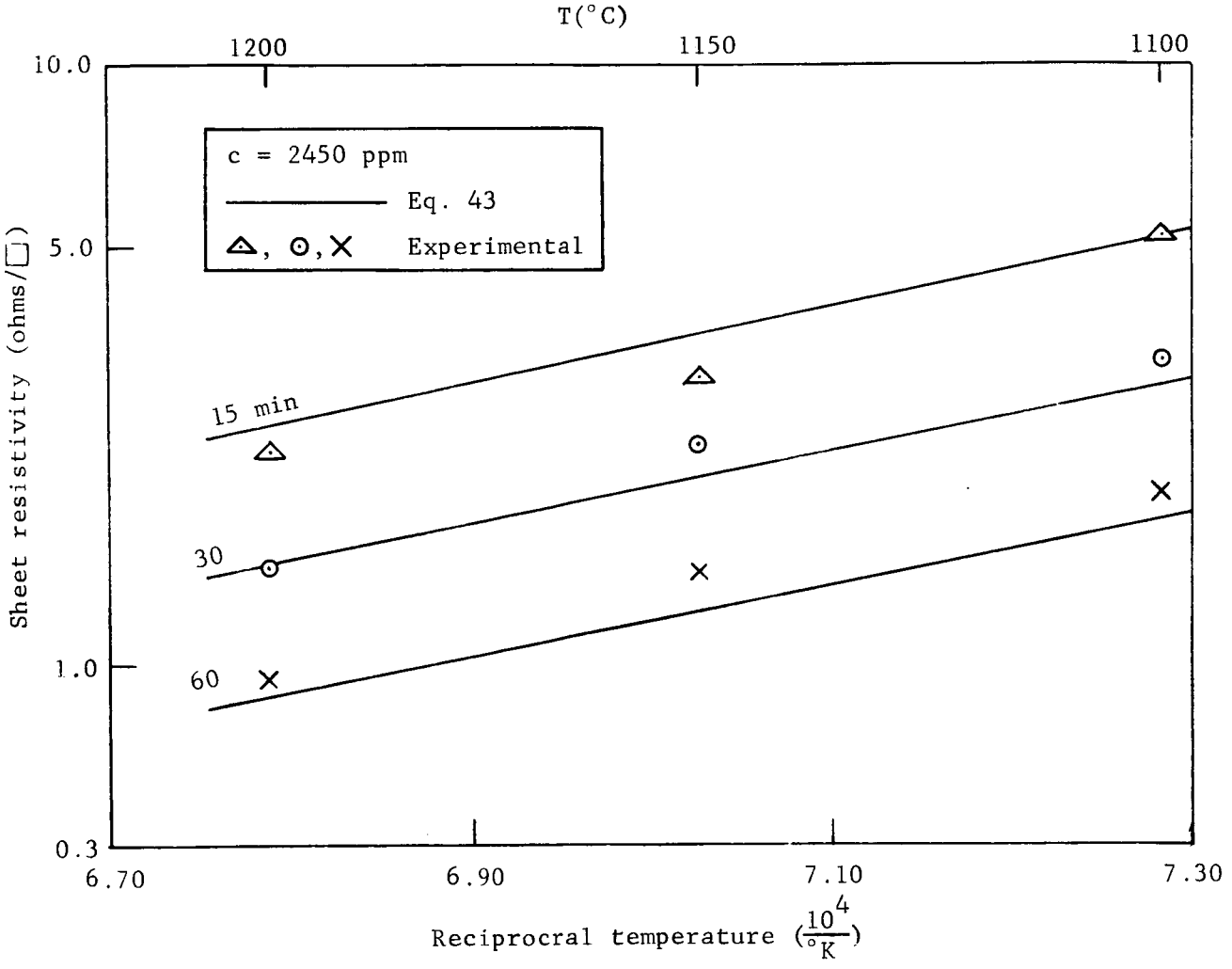

Fig. 16. A comparison of sheet resistivity as predicted by Eq. 43 and that observed (aveg. top surface data, Table 1) for the highest value of impurity concentration

equation under the appropriate boundary conditions made in Eq. 25 is probably not justified. A next step is to re-examine these solutions to decide the type of correction needed in the very simple model. This same data, already available, can be fitted to any new model and the improvement immediately checked.

Equation 37, describing the tentative relationship between junction breakdown voltage and the time and temperature of diffusion, shows only a fair correlation between the predicted breakdown voltage and the actual. The maximum voltage measured was 51 volts ($\ln 51 \sim 3.93$); the minimum, 35 volts ($\ln 35 \sim 3.56$). The range of $\ln V_B$ is thus about 0.37; the standard deviation in $\ln V_B$ of 0.073 represents an uncertainty of almost 20% in V_B (not $\ln V_B$). In addition the multiple correlation coefficient indicates that substantially less than 50% of the data are explained by the proposed model.

The models for reverse current, Eqs. 38 and 39, show significantly poorer fits. The standard deviation is of the same order of magnitude as the variable itself and the multiple correlation coefficient is unacceptably low. The obvious conclusion is that the models are inadequate, and from the lack of any well established dependence between I_R and the product $x_j\rho_s$ it appears likely that other variables, not at present controlled or measured, are of prime significance.

The difference between the diodes labelled L and those labelled S is one of diameter only. As shown in Fig. 8, both diodes are circular but the diameter of the L units is 9 mils and that of the S units, 4.5 mils. No significant difference in $V_{(BR)}$ could be detected between the L and the S units. $I_{R_{(L)}}$, however, generally seemed to be twice that

of $I_{R_{(S)}}$, as indicated in Eqs. 38 and 39. This observation suggests that the geometrical variable of importance is perimeter rather than area and that the source of the added reverse current observed with the large units occurs at the surface. Since only bulk parameters have been included in Eqs. 38 and 39, and these models have been shown to be inadequate, a reasonable next step is to incorporate a parameter describing the surface contribution.

Dependence of reverse current on the radial position of the wafer was clearly evident on only one wafer. The reverse current in this case, decreased with radial distance, the outside diodes having the lowest current. Breakdown voltage on this same wafer, as well as all others, seemed independent of radial position.

The advantages gained by modeling reverse current at 200°C instead of room temperature are shown in Fig. 17. The room temperature measurements of I_R are shown in Fig. 17a for diode positions 1s through 9s. In Fig. 17b the same measurements are shown when measured at 200°C. Obviously the distribution of reverse currents has considerably narrowed, indicating that a single mechanism causing current flow may predominate at this temperature. At any rate, measuring a typical value of I_R is no longer as hopeless as it appeared at room temperature.

Fig. 17c shows the 200°C measurements on the large diodes 1L through 9L.

A second group of wafers was run through the factorial diffusion experiment, in which the quartz diffusion tube was replaced by an alumina tube. Raw data recorded on these wafers is given in Table 3. Models were fitted for x_j and ρ_s, viz. (units are given in Table 2),

Table 3

Raw Data from Second Diffusion Experiment

Wafer No.	Temp. (°C)	Concentration (ppm)	Time (Min.)	Aveg. ρ_s (Ω/□)		Median ρ_s (Ω/□)		Junction Depth (A)		Aveg. Layer Resistivity (ohm-cm)$\times 10^{-4}$	
				Top	Bot	Top	Bot	Top	Bot	Top	Bot
B-68	1100	35	15	177	133	172					
B-82	1100	35	30	133	160	120	135	5100	7600	68	114
B-81	1100	35	60	39	42	37	38.5	12100	10200	47.2	4.3
B-63	1100	35	120	21	15	10.8	14	19800	19100	41.6	28.7
B-67	1100	250	15	9.7	8.6	9.9	8.35	15800	12700	15.3	1.09
B-73	1100	250	35	5.4	5.1	5.95	5.05	18700	18000	1.02	.92
B-72	1100	250	60	4	3.4	4	3.35	23300	25500	9.3	9
B-61	1100	250	15	10.15	8.42	10.1	8.3	15200	10000	15.4	8.42
B-78	1100	2450	15	3.42	2.97	3.4	2.97	18500	17800	6.33	5.28
B-71	1100	2450	30	2.25	1.92	2.22	1.9	26600	22200	6	4.16
B-46	1100	2450	60	1.71	1.42	1.68	1.42	32500	30300	5.56	4.68
B-2	1150	3.5	15	415	348	425	340	6100	6400	253	2.23
B-70	1150	3.5	30					7600	9600		
B-79	1150	3.5	60	83	60	82.5	62.5	16200	15600	134	94
B-66	1150	3.5	30	160	129	170	125	9200	7400	147	96
B-32	1150	250	15	7.7	5.7	7.55	5.7	16000	17800	12.3	10.03
B-60	1150	250	30	5.37	4.5	5.4	4.5	25000	23300	13.4	10.05
B-87	1150	250	30	5.08	425	5.0	4.2	23100	20200	11.8	8.6
B-80	1150	250	60	3.46	2.7	3.35	2.7	31400	32400	10.9	9.8
B-74	1150	2450	15	2.79	7.4	2.73	2.4	23100	24800	6.45	5.95
B-88	1150	2450	30	1.83	1.46	1.80	1.45	35600	33000	6.6	4.8
B-47	1150	2450	60	1.27	1	1.21	1	45600	35300	5.8	3.53
B-42	1200	35	15	454	359	455	325	6700	9400	305	240
B-50	1200	35	30								
B-17	1200	35	30	240	109	235	105	17500	13200	420	144
B-43	1200	35	60	65	70.5	62	69	22800	22300	148	157
B-36	1200	250	15	1085	9.1	9.5	9.25	23700	21000	25.7	19.2
B-19	1200	250	35	5.64	4.24	5.6	4.2	34100	33000	19.4	17.8
A-73	1200	250	60	4.05	3.15	3.97	3.15	43300	41600	17.4	13.2
A-78	1200	2450	15	2.3	1.93	2.3	1.9	33000	22300	1.7	4.3
A-71	1200	2450	30	1.35	1.15	1.32	1.15	44000	46500	5.95	5.35
A-83	1200	2450	60	.88	.76	.855	.76	57600	44200	5.06	3.35
A-75	1200	35	15	481	406	480	395	10000	9000	481	365
A-79	1150	35	30	461	491	450	515	9200	9400	425	364

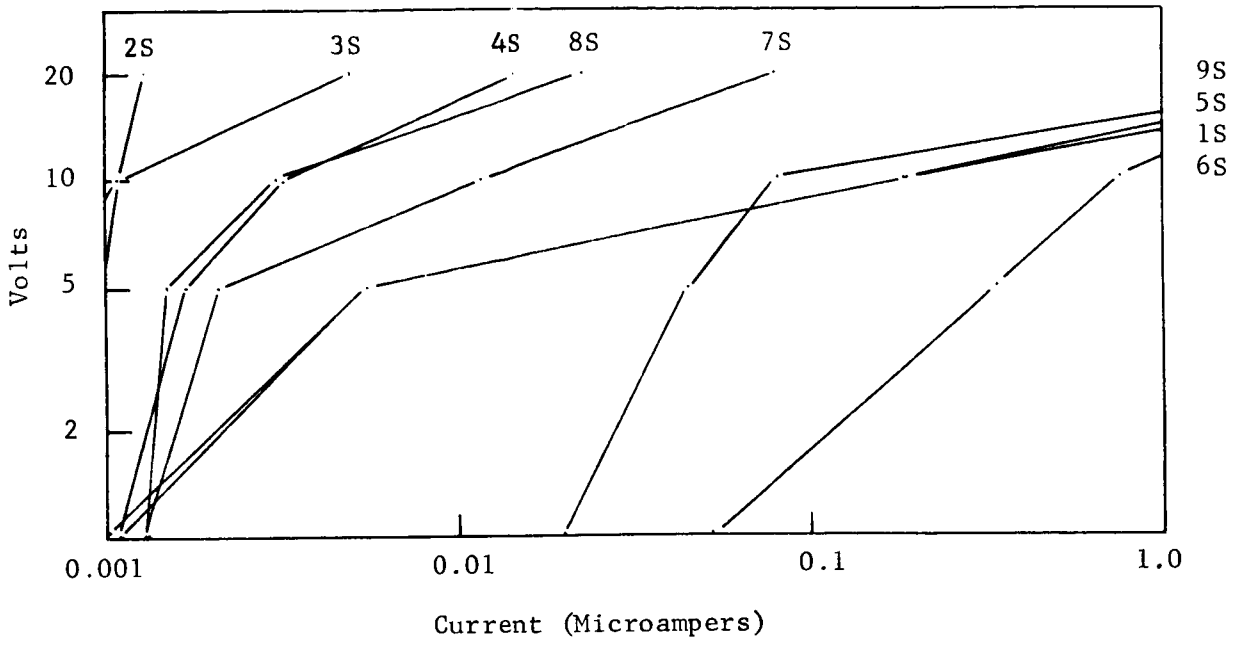

a. Small diodes at room temperature

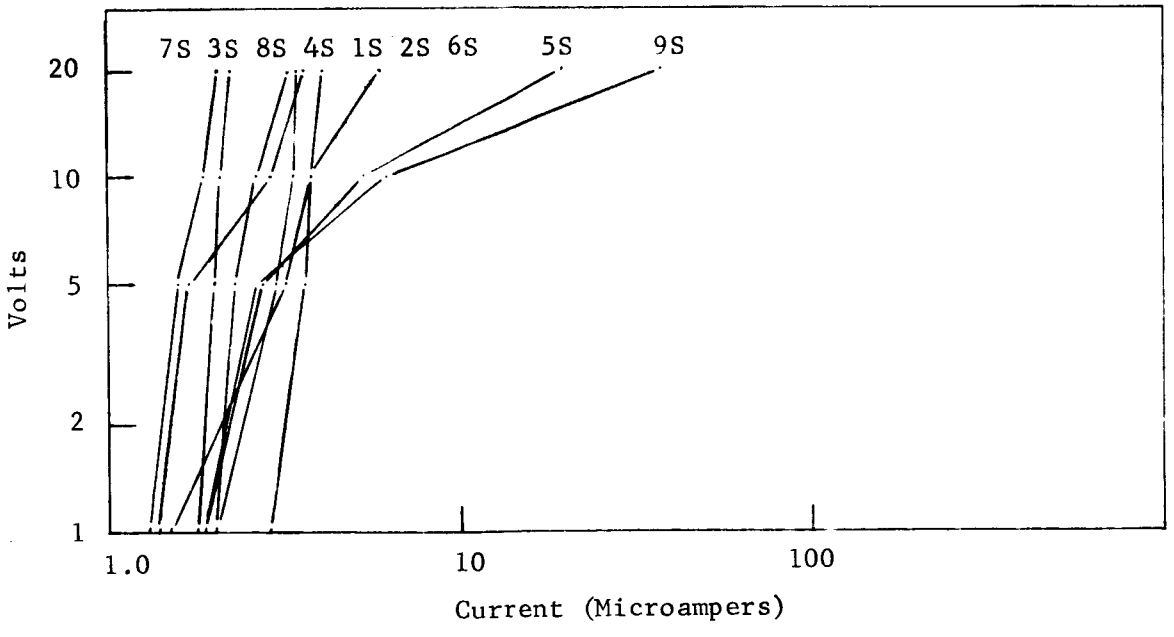

b. Same diodes at 200°C

Fig. 17. Typical diode I-V characteristics

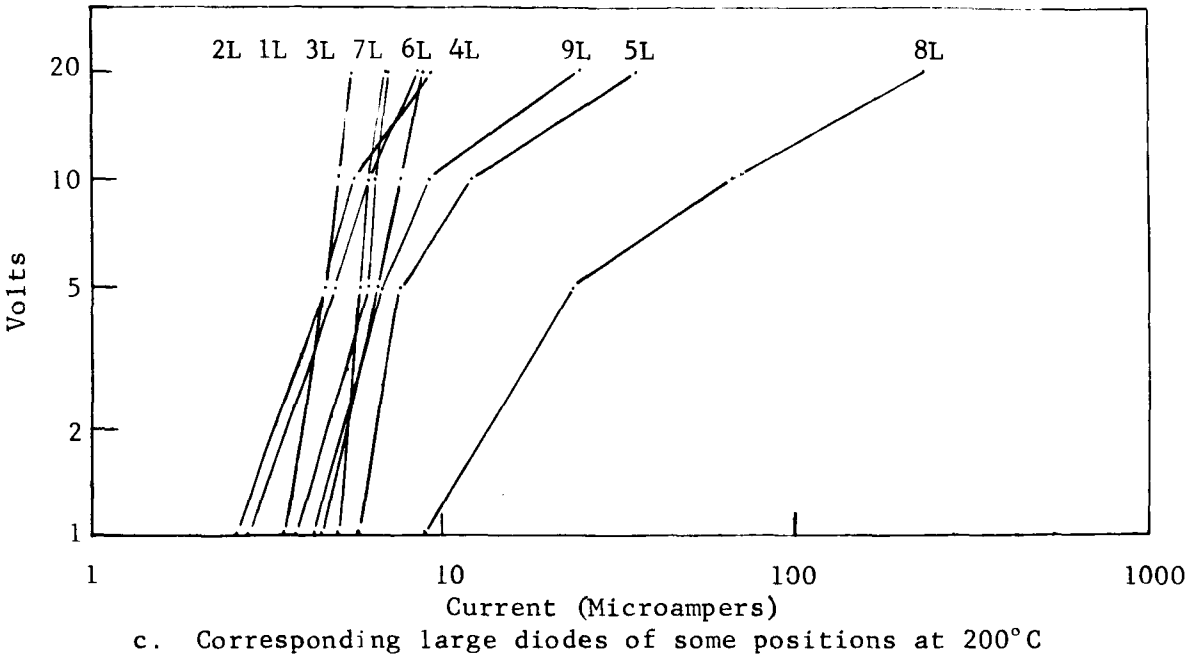

c. Corresponding large diodes of some positions at 200°C

Fig. 17 (continued). Typical diode I-V characteristics

$$x_j = 19.964\ t^{0.43}\ e^{-\frac{9700}{T}}\ (\ln c - 1.4)\ A \qquad (44)$$

$$R \simeq 0.97 \qquad s = 2756$$

$$\rho_s = \frac{9.46 \times 10^4\ t^{-1.5}\ e^{\frac{5000}{T}}}{c(\ln c - 0.5)}\ \text{ohms/}\square \qquad (45)$$

$$R \simeq 0.92 \qquad s = 59.4$$

Both the standard deviation and the multiple correlation coefficient are comparable to that previously calculated (Eqs. 35 and 36); therefore, no improvement in statistical fit has been realized in switching to the alumina diffusion tube. More significant, however, is the variation in the values of the fitted coefficients between the two sets of data. These numbers are heavily influenced by the high values of sheet resistivity and a comparison of Table 1 and Table 3 shows that reproducibility

in this range of operation is poor. There is much better agreement within a single set of data than between the two separate sets (again this statement applies to low values of c primarily; at high values, the data agree much better). Tube history effects are a possible explanation.

No electrical properties were measured on the diodes formed on these wafers.

The functional form of the models fitted so far do not predict the observed dependence of sheet resistivity upon temperature at low values of c (both c = 35 ppm and c = 250 ppm). At the highest value of c the functional form of the model fits quite well. Reproducibility is also the best in this range of operation. These observations strengthen the argument for operation at the limiting solid solubility of phosphorus in silicon, achieving control of junction depth and sheet resistivity by controlling the time and temperature of not only a standard impurity introducing diffusion cycle but of a subsequent, redistribution cycle as well, in which the wafer is heated in an impurity free atmosphere and only the impurities already present are available to participate in the diffusion process. This method is the "two-step" diffusion method commonly employed in industry today. Its major advantage is that the value of impurity concentration at the surface is determined by the limiting solid solubility of the impurity in silicon at the temperature of diffusion rather than by the concentration of impurity in the gas phase adjacent to the silicon surface. However, in modeling such a diffusion process--that is, in writing down the functional relationship

describing how the sheet resistivity and junction depth are dependent upon the various times and temperatures employed--the number of independent variables is increased (at least two independent times and temperatures are required--one each for the deposition cycle and one each for the redistribution cycle) and most likely not all important variables are yet known (the amount of oxide formed during a boron redistribution, for example, influences the sheet resistivity and junction depth drastically [Ref. 3]). Empirical curves exist, of course, which permit good control of the diffusion but these curves are usually unique to specific manufacturers for a specific type of diffused layer and sometimes are restricted to specific furnaces! Already the models developed for the one step diffusion process seem more general and perhaps more informative than anything that can be written down to describe the two-step process. The major problem of course is control of the variable c at low values. More exploration of methods for improving this control seem warranted before abandoning the one step method as irreproducible.

5. Conclusions and Recommendations

The data evaluation to date indicates that the functional form of the model relating junction depth to the time, temperature, and impurity concentration during diffusion is probably adequate (for interpolation) as it now stands (Eqs. 21, 35). The model for sheet resistivity in terms of these same parameters (Eqs. 29, 43) is good at the highest value of impurity concentration investigated (2450 ppm) but not at the lowest (35 ppm) or intermediate value (250 ppm). Some additional terms or factors modifying the time-temperature dependence at low values of c are needed.

Reproducibility, particularly of ρ_s, is inadequate at low value of c. Better means of measuring the value of c during diffusion are desirable. The present method relies on external metering of the gas flows into the tube for control of c; a more direct measurement of the c value in the diffusion tube, such as a phosphorus chemical-potential detector, is needed. To be of maximum benefit this detector should read continuously and come to equilibrium with the phosphorus content of the gas flow in a time small compared with the time of diffusion. A simple resistance theomometer is suitable provided: (1) its resistance is sensitive to P_2O_5 impurities in the concentration ranges of interest; and (2) the diffusion coefficient of P_2O_5 in the thermometer material is sufficiently high so as to achieve an equilibrium rapidly (1 to 5 minutes maximum).

The models for both $V_{(BR)}$ and I_R are not adequate and probably incomplete in that significant variables are being neglected. The surface contribution in particular has been ignored. To account for surface effects some unambiguous measure of its contribution to both

reverse current and breakdown voltage must be found. Although the quantitative theory is not yet developed, the measure of the flat band voltage of the oxidized silicon immediately adjacent to the outcropping of the planar p-n junction promises to be very informative of surface charge and hence surface contributions to current flow and breakdown voltage. The flat band voltage measurement can be made by adding an insulated electrode to the present diode pattern:

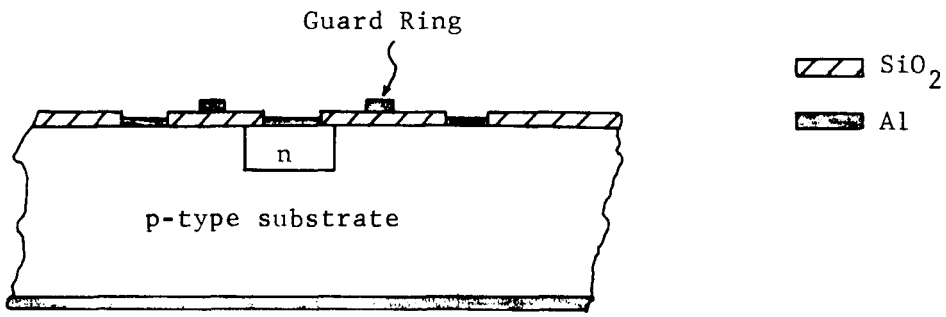

The capacitance between the guard ring and the substrate can be measured as a function of voltage. Both the zero voltage capacitance and the flat band voltage are deducible from such measurements. Oxide thickness can be independently measured by color or interference techniques.

Specific next steps in the program are the concurrent investigations of:

1. Methods of improving control over diffusions at impurity concentrations of 35 ppm and less. A direct measurement of P_2O_5 concentration in the neighborhood of the silicon being diffused is quite desirable.
2. Significant surface related measurements to incorporate into the models for breakdown voltage and reverse current of a

planar, diffused diode. Control of any measurement so identified in terms of processing variables is an important but subsequent problem.

3. Models which are likely to be suitable over a wider range and to be more exact than the present ones.

References

1. Research Triangle Institute, "Diffusion of Silicon from a Phosphine Gas Source," Solid State Laboratory Technical Note No. 3, October 1963.

2. Research Triangle Institute, Integrated Silicon Device Technology, Vol. IV----Diffusion, ASD-TDR-63-316, Vol IV, Contract No. AF 33 (657)-10340, Durham, N. C., February 1964 (U) AD 603 716.

3. F. M. Smits, "Formation of Junction Structures by Solid State Diffusion," Proc. IRE 46, June 1958, pp. 1049-1061.

4. F. M. Smits and R. C. Miller, "Rate Limitation at the Surface for Impurity Diffusion in Semiconductors," Phys. Rev. 104, Dec. 1956, pp. 1242-1245.

5. H. S. Veloric, M. B. Prince, and M. J. Eder, "Avalanche Breakdown Voltage in Silicon Diffused p-n Junctions as a Function of Impurity Gradient," J. Appl. Phys. 27, Aug. 1956, pp. 895-899.

6. T. Chung, "Graphical Analysis of the Parameters Affecting the Voltage Tolerance in Silicon p-n or n-p Junctions," Solid-State Electronics 7, Sept. 1964, pp. 687-693.

7. C. T. Sah, "Effect of Surface Recombination and Channel on p-n Junction and Transistor Characteristics," IRE Trans. Elect. Dev., ED-9, Jan. 1962, pp. 94-108.

8. Research Triangle Institute, "Direct Dynamic Observations of Impurity Flow Patterns During Gas-Source Boron Diffusions of Silicon," Solid State Laboratory Technical Note No. 11, October 1964.

9. Research Triangle Institute, Integrated Silicon Device Technology, Vol. III----Photoengraving, ASD-TDR-63-316, Vol. III, Contract No. AF 33(657)-10340, Durham, N. C., January 1964 (U) AD 603 715.

10. Research Triangle Institute, Integrated Silicon Device Technology, Vol. VII----Oxidation, ASD-TDR-63-316, Vol VII, Contract No. AF 33 (615)-1998, Durham, N. C., to be issued.

11. B. McDonald and A. Goetzberger, "Measurement of the Depth of Diffused Layers in Silicon by the Grooving Method," J. Electrochem. Soc. 109, February 1962, pp. 141-144.